UNIVERSITY OF CRETE
DEPARTMENT OF CHEMISTRY

GENERAL POSTGRADUATE PROGRAMME IN CHEMISTRY

LABORATORY OF TISSUE ENGINEERING - REGENERATIVE MEDICINE AND IMMUNO-ENGINEERING (IESL-FORTH)

MASTER THESIS

The effect of physicochemical properties of polycaprolactone (PCL) scaffolds on the adhesion, proliferation and differentiation of mouse Mesenchymal Stem Cells (MSCs)

TSOUTSA MARIA ELENI

Master Thesis Supervisors:

Prof. Athanassios Coutsolelos

Dr. Anthi Ranella

HERAKLION, CRETE,

MARCH 2021

INSTITUTE OF ELECTRONIC STRUCTURE AND LASER

ΤΜΗΜΑ ΧΗΜΕΙΑΣ

ΓΕΝΙΚΟ ΜΕΤΑΠΤΥΧΙΑΚΟ ΠΡΟΓΡΑΜΜΑ ΧΗΜΕΙΑΣ

ΕΡΓΑΣΤΗΡΙΟ ΜΗΧΑΝΙΚΗΣ ΙΣΤΩΝ-ΑΝΑΓΕΝΝΗΤΙΚΗΣ ΙΑΤΡΙΚΗΣ ΚΑΙ ΑΝΟΣΟ-ΜΗΧΑΝΙΚΗΣ(ΙΗΔΛ-ΙΤΕ)

ΜΕΤΑΠΤΥΧΙΑΚΟ ΔΙΠΛΩΜΑ ΕΙΔΙΚΕΥΣΗΣ

Η επίδραση των φυσικοχημικών ιδιοτήτων ικριωμάτων πολυκαπρολακτόνης στην προσκόλληση, τον πολλαπλασιασμό και τη διαφοροποίηση μεσεγχυματικών βλαστικών κυττάρων ποντικού

ΤΣΟΥΤΣΑ ΜΑΡΙΑ ΕΛΕΝΗ

ΥΠΕΥΘΥΝΟΙ ΚΑΘΗΓΗΤΕΣ:

Καθ. ΑΘΑΝΑΣΙΟΣ ΚΟΥΤΣΟΛΕΛΟΣ

Δρ. ΑΝΘΗ ΡΑΝΕΛΛΑ

ΗΡΑΚΛΕΙΟ, ΚΡΗΤΗ

ΜΑΡΤΙΟΣ 2021

INSTITUTE OF ELECTRONIC STRUCTURE AND LASER

Στη γιαγιά Ζωή

Examination committee

1) Coutsolelos Athanassios

Professor of Chemistry Department, University of Crete

2) Ranella Anthi

Assistant Researcher, Institute of Electronic Structure and Laser, Foundation for Research and Technology

3) Stratakis Emmanuel

Research Director, Institute of Electronic Structure and Laser, Foundation for Research and Technology

ACKNOWLEDGEMENTS

I'm deeply grateful to my supervisor, Dr. Ranella Anthi, who gave me the opportunity to work in the laboratory of Tissue Engineering-Regenerative Medicine and Immuno-engineering (TERMIM), for providing this interesting and challenging topic and for advising me during my master thesis. Also, I would like to thank Prof. Coutsolelos Athanassios for accepting this collaboration and Dr. Stratakis Emmanuel for being in the examination committee of my master thesis.

Furthermore, I would like to express my full appreciation to Dr. Paraskevi Kavatzikidou for mentoring me both in experimental and personal part. This work would not be possible without her aid and I would like to thank her for her invaluable help and support and for answering to my messages 24/7!

Also, I would like to thank each member of TERMIM group separately. They were very kind, willing to teach me how to work in the lab from the first moment and I hope I was a pleasant company for them. It's my honor to be a member of this group!

Special thanks to Aleka Manousaki for the infinite SEM images and for her patience in my annoying demands.

Also, I would like to thank Anna Karagiannaki and Despina Angelaki for the master Si substrates and Alexandros Mimidis, who helped me with the handling of contact angle instrument.

Finally, I would like to thank my family for their endless support in each of my choices. Even though they were many kilometers away, they were always by my side.

Thank you all!

CURRICULUM VITAE

PERSONAL INFORMATION

First name: Maria Eleni

Last name: Tsoutsa

Date of birth: 29/09/1996

Telephone number: (+30) 6975621328

E-mail address: chemp1028@edu.chemistry.uoc.gr

EDUCATION

M.Sc. in Physical Chemistry – Advanced Materials Mar. 2019-Mar.2021

Department of Chemistry, University of Crete

- Master thesis: "*The effect of physicochemical properties of polycaprolactone (PCL) scaffolds on the adhesion, proliferation and differentiation of mouse Mesenchymal Stem Cells (MSCs)"* (Supervisors: Prof. Athanassios Coutsolelos, Dr. Anthi Ranella)

B.Sc. in Chemistry Sept. 2014-Mar. 2019

Department of Chemistry, University of Crete

- Bachelor thesis: "*Synthesis of porphyrine hybrid for use in perovskite solar cells*" (Supervisor: Prof. Athanassios G. Coutsolelos)

SKILLS AND TECHNIQUES

- Column chromatography
- UV/VIS Spectrophotometer
- Thin layer chromatography (TLC)
- Mass spectrometry [Matrix-Assisted Laser Desorption Ionization-Time of Flight (MALDI-TOF)]
- Cell cultures
- ELISA microplate reader
- Water contact angle

CONFERENCES

- 21st Postgraduates' Conference in Chemistry, University of Crete, Heraklion, Crete, Greece, 17-19 May 2019

SUMMER SCHOOLS

- V Summer School "Photonics meets Biology", FORTH, Heraklion, Crete, Greece, 16 September-20 September 2019

LANGUAGES

- Greek (Native Language)
- English (Certificate of English Language Proficiency, Level C2, Michigan State University)

INTERESTS

- Tissue engineering
- Biomaterials
- Biodegradable polymers

TEACHING EXPERIENCE

- Teaching assistant at the undergraduate Laboratory of Inorganic Chemistry, Department of Chemistry, University of Crete, Greece (Oct. 2019 - Mar.2020)

SOFTWARE

- Microsoft Office
- OriginPro
- Fiji ImageJ
- Chemdraw

ABSTRACT

The increasing demand for biocompatible bone substitutes has made it a priority to tissue engineering and regenerative medicine scientists. Last decades, there is an interest for topographic features on the implants, which have been proven to mechanically regulate cell behavior and functions. The soft lithography techniques provide the opportunity to replicate accurately cell culture patterned surfaces on polymers of interest, where the effect of various topographical cues on cellular functions can be studied. The most studied synthetic polymers in bone tissue regeneration are aliphatic polyesters, due to their advantage of being easily tailored according to the demands. However, there are still some concerns about osteoconductivity, absorption timing and local pH alterations to polymers' surfaces.

In this study, the material of interest is the polycaprolactone (PCL), a biodegradable synthetic polymer that has been widely used to produce 3D scaffolds due to its biocompatibility, biodegradability, structural stability and excellent mechanical properties. Cell culture studies were carried out using mouse Mesenchymal Stem Cells (mMSCs), an important cell source in tissue engineering due to their ability to self-renew, proliferate, and differentiate into a wide range of tissue-specific lineages, including chondrogenic, adipogenic and osteogenic lineages. The aim of this study is to investigate the effect of patterned and non-patterned (flat) PCL surfaces on mMSCs morphology, adhesion, proliferation and osteogenic differentiation.

In an attempt to enhance the cell attachment properties of PCL, we have used ultrafast laser patterned surfaces. Ultrafast pulsed laser irradiation is considered as a simple, precise and effective microfabrication method to produce structures of controlled geometry and pattern regularity. In our study, two types of PCL patterned surfaces (low and high roughness) and a PCL non-patterned (flat) surface were fabricated via soft lithography method, by using such patterned masters. Their topographical features and surface wettability were assessed by Scanning Electron Microscopy (SEM) and static contact angle measurements. In order to study the effect of surface properties on cell behavior, the MSCs were cultured on PCL patterned and non-patterned substrates.

Specifically, the effect of topography on cytoskeleton organization (cell shape), the focal adhesion activity and the cell mechanotransduction were studied. Furthermore, the ability of MSCs cultured on patterned PCL surfaces with various stiffness and topographies to differentiate toward osteogenic lineage and to produce a mineralized matrix were evaluated. It is assumed that our tailor-made PCL micro-environments give the opportunity to affect the cellular behavior and seem to be promising in the field of bone tissue engineering and regenerative medicine in the future.

Keywords: tissue engineering, soft lithography, topography, mMSCs, polycaprolactone, cell adhesion, Yes-associated protein (YAP), osteogenic differentiation, mechanotransduction

ΠΕΡΙΛΗΨΗ

Η αυξανόμενη ζήτηση για βιοσυμβατά οστικά μοσχεύματα τα καθιστά προτεραιότητα για τους επιστήμονες της μηχανικής ιστών και της αναγεννητικής ιατρικής. Τις τελευταίες δεκαετίες, υπάρχει αρκετό ενδιαφέρον για εμφυτεύματα με συγκεκριμένες τοπογραφίες, οι οποίες έχει αποδειχθεί ότι ρυθμίζουν μηχανικά τη συμπεριφορά και τις λειτουργίες των κυττάρων. Οι τεχνικές της μαλακής λιθογραφίας παρέχουν την δυνατότητα πιστής αναπαραγωγής τοπογραφιών πάνω σε επιφάνειες πολυμερών. Πάνω στις πολυμερικές αυτές επιφάνειες μπορούν να πραγματοποιηθούν κυτταρικές καλλιέργειες και να μελετηθεί η επίδραση των τοπογραφικών ερεθισμάτων στις κυτταρικές λειτουργίες. Τα πιο μελετημένα συνθετικά πολυμερή στο πεδίο της αναγέννησης οστικών ιστών είναι οι αλειφατικοί πολυεστέρες, λόγω του πλεονεκτήματός τους να επεξεργάζονται εύκολα και να προσαρμόζονται σύμφωνα με τις ανάγκες. Παρόλα αυτά, εξακολουθούν να υπάρχουν ορισμένα θέματα που δεν έχουν εξακριβωθεί πλήρως και σχετίζονται με την οστεοαγωγιμότητα, το χρονικό διάστημα απορρόφησης των ενθεμάτων και τις τυχόν μεταβολές στις επιφάνειες των πολυμερών που μπορούν να προκληθούν από μεταβολές του pH.

Σε αυτήν τη διατριβή, το υλικό που επιλέχθηκε για να μελετηθεί είναι η πολυκαπρολακτόνη (PCL), ένα βιοαποικοδομήσιμο συνθετικό πολυμερές που έχει χρησιμοποιηθεί ευρέως για την παραγωγή τρισδιάστατων ικριωμάτων λόγω της βιοσυμβατότητας, της βιοαποικοδομησιμότητας, της δομικής σταθερότητας και των εξαιρετικών μηχανικών ιδιοτήτων του. Διεξήχθησαν, επίσης, κυτταρικές καλλιέργειες με μεσεγχυματικά βλαστικά κύτταρα ποντικού (mMSCs), τα οποία αποτελούν μια σημαντική πηγή κυττάρων για την μηχανική ιστών λόγω της ικανότητάς τους να αυτό-ανανεώνονται, να πολλαπλασιάζονται και να διαφοροποιούνται ως προς ένα ευρύ φάσμα κυτταρικών κατηγοριών, όπως τα χονδροκύτταρα, τα λιποκύτταρα και τα οστεοκύτταρα. Στόχος της συγκεκριμένης διατριβής είναι η μελέτη της επίδρασης επιφανειών πολυκαπρολακτόνης με τοπογραφία (χαμηλής και υψηλής τραχύτητας) και χωρίς τοπογραφία (επίπεδες) στη μορφολογία, την προσκόλληση, τον πολλαπλασιασμό και την διαφοροποίηση των mMSCs προς οστεοκύτταρα.

Προκειμένου να αυξήσουμε την προσκόλληση των κυττάρων στις επιφάνειες πολυκαπρολακτόνης, χρησιμοποιήθηκαν ειδικά σχεδιασμένες επιφάνειες με λέιζερ υπερβραχέος παλμού(ultrafast laser). Η ακτινοβόληση επιφανειών με λέιζερ υπερβραχέος παλμού θεωρείται απλή, ακριβής και αποτελεσματική μέθοδος παραγωγής δομών ελεγχόμενης γεωμετρίας. Σε αυτή τη μελέτη, δημιουργήθηκαν τρεις τύποι επιφανειών πολυκαπρολακτόνης με τη μέθοδο της μαλακής λιθογραφίας: επίπεδες, χαμηλής τραχύτητας και υψηλής τραχύτητας. Οι επιφάνειες αυτές αποτελούν πιστή αναπαραγωγή των εκμαγείων που χαράχθηκαν με ultrafast pulsed laser. Τα τοπογραφικά χαρακτηριστικά και η ικανότητα διαβροχής των επιφανειών αυτών αξιολογήθηκαν με ηλεκτρονική

μικροσκοπία σάρωσης (SEM) και με μετρήσεις γωνίας επαφής. Προκειμένου να μελετηθεί η επίδραση των ιδιοτήτων των επιφανειών στη συμπεριφορά των κυττάρων, τα MSCs καλλιεργήθηκαν σε υποστρώματα πολυκαπρολακτόνης με τοπογραφία (χαμηλής και υψηλής τραχύτητας) και χωρίς τοπογραφία (επίπεδα).

Συγκεκριμένα, εξετάστηκε η επίδραση της τοπογραφίας στην οργάνωση του κυτταροσκελετού (σχήμα του κυττάρου), στην προσκόλληση των κυττάρων και στη μηχανική μεταγωγή σημάτων σε αυτά. Επιπλέον, μελετήθηκε η ικανότητα των MSCs, που καλλιεργήθηκαν σε επιφάνειες πολυκαπρολακτόνης με διαφορετικές τοπογραφίες και ένα ευρύ φάσμα τραχύτητας, να διαφοροποιηθούν προς οστεοκύτταρα και να παράγουν ασβέστιο. Θεωρείται ότι τα ειδικά σχεδιασμένα μικρο-περιβάλλοντα πολυκαπρολακτόνης μας δίνουν την δυνατότητα να επηρεάσουμε την κυτταρική συμπεριφορά και φαίνεται να είναι πολλά υποσχόμενα για τον τομέα της μηχανικής οστών και της αναγεννητικής ιατρικής στο μέλλον.

Λέξεις-Κλειδιά: μηχανική ιστών, μαλακή λιθογραφία, τοπογραφία, μεσεγχυματικά βλαστικά κύτταρα ποντικού (mMSCs), πολυκαπρολακτόνη, προσκόλληση κυττάρων, Yes-associated protein (YAP), οστεοκύτταρα, μηχανική μεταγωγή

Contents

LIST OF FIGURES

LIST OF TABLES

ABBREVIATIONS

Ab	Antibody
ALP	Alkaline Phosphatace
ARS	Alizarin Red S
DAPI	4,6-diamidino-2-phenylindole
DMEM	Dulbecco's modified Eagle's medium
ECM	Extracellular Matrix
ELISA	Enzyme-linked Immunosorbent Assay
EtOH	Ethanol
FA	Focal Adhesion
FBS	Fetal Bovine Serum
GDA	Glutaraldehyde
HDMS	Hexamethyldisilazane
MeOH	Methanol
MSCs	Mesenchymal Stem Cells
OD	Optical Density
PBS	Phosphate Buffered Saline
PCL	Polycaprolactone
PFA	Paraformaldehyde
PLGA	Poly(Lactic-co-Glycolic Acid)
PS	Penicillin/Streptomycin solution
RT	Room Temperature
SCB	Sodium Cacodylate Buffer
SEM	Scanning Electron Microscope
TCP	Tissue Culture Plastic
TE	Tissue engineering
YAP	Yes-associated protein

1. Introduction

1.1 Tissue engineering and regenerative medicine

Tissue and organ failure have traditionally been treated by the implementation of autografts or allografts. In 1954, Dr. Joseph Murray performed the first transplant in a human when he transferred a kidney from one identical twin to another.[1] Although organ transplantation is the only effective treatment in cases of injury, insufficiency, malfunction or deformity of an organ, there are limitations and the most dominant of them were the lack of donors, the probability of immune rejection and pathogen infection. Furthermore, chronic diseases are on the rise and the process of tissue regeneration becomes urgent. There is therefore an interest in evolution of extraneous repair by replacing tissues via stimulating tissue formation and regeneration. So, the need created for new technologies that led to the creation of Tissue Engineering (TE) and Regenerative Medicine. The main goal of Tissue Engineering is to restore lost or damaged tissue involving a combination of three factors: scaffolds, cells, and growth factors.[2] Scaffolds are either temporary or permanent matrices responsible for supporting and regulating the growth of new tissue. Regenerative medicine is the branch of medicine that develops methods to regrow, repair or replace damaged or diseased cells, organs or tissues. Regenerative medicine includes the generation and use of therapeutic stem cells, tissue engineering and the production of artificial organs[3]. Tissue engineering and regenerative medicine promise to treat diverse diseases that are currently intractable.

The current strategy for tissue engineering typically entails the *ex vivo* expansion of multipotential cell populations, such as mesenchymal stem cells (MSCs), followed by their transplantation into damaged areas (Fig.1). Due to their unique regenerative potential and immunomodulatory properties, MSCs hold great promise in tissue engineering and reconstructive therapies, not only directly participating in wound healing and regeneration but also modulating the host foreign-body immunogenic reaction to transplants. These cells are able to be transplanted within a biodegradable 3D biomaterial-cell construct that mimics the requisite extracellular milieu providing physical and chemical cues for cell-driven tissue development and regeneration. It is now established that approaches to engineer biological tissues must integrate and approximate the mechanics, both static and dynamic, of native tissues. Although a wide variety of therapeutic strategies, based on different types of biomaterials and stem cells, have been and are still being explored, in practice, modern tissue engineering is not an easily accessible approach to achieve regeneration in a clinical setting, because there are biological, technical and regulatory hurdles that have not being overcome yet.[4]

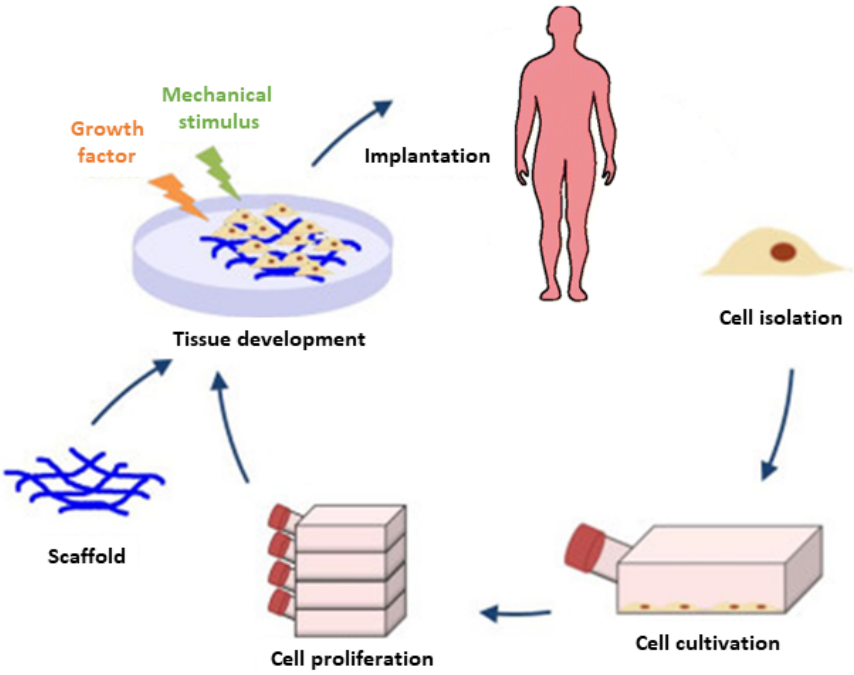

Figure 1: Schematic representation of tissue engineering stages[1]

1.2 Biomaterials in tissue engineering

Living tissues are materials engineered by nature itself to have a specific structure that affects cell properties and drives all consequent biological events. A tissue substitute must be biomechanically able to fulfill the functions of the tissue it replaces and, as such, should have mechanics similar to those of the native tissue. Tissue engineering tries to replicate living tissues functions by designing the structure of a biomaterial to recapitulate a predetermined cell response. The basic role of biomaterials in tissue engineering is to provide temporary mechanical support and mass transport to encourage cell adhesion, proliferation, and differentiation and to control the size and shape of the regenerated tissue. [5,6] These matrices should have a desirable architecture that provides functionality and supports tissue regrowth until sufficient new tissue is formed.[4]

Living cells grow and function while being tightly associated with the diverse connective tissue components that form the *extracellular matrix* (ECM), which provides structural support for cells residing in a tissue to attach, grow, migrate and respond to signals.[7] ECM is a complex fibrous network with micro-/nano-hierarchical features and tunable elastic properties. It is well recognized that cells receive cues from their extracellular environment from multiple sources

[1] https://enacademic.com/dic.nsf/enwiki/184345

and these biochemical components have a substantial impact on cell behavior.[8,9,10]

One of the main goals in the field of biomaterials and tissue engineering is to identify and utilize non biological cues. This control of cellular response includes aspects such as cell adhesion, migration, proliferation, cell-to-cell communication, and expression of a desired phenotype.[11] The last decade, many material science approaches to control cellular response are showing significant promise, however, there is still a lack of fundamental understanding on how these non-biological cues influence cell−biomaterial interactions. These cues include surface properties such as chemistry, topography, charge, interfacial free energy, wettability, stiffness, etc. (Fig.2). Mechanobiology is an emerging field investigating the translation of physical forces into molecular biological signals.

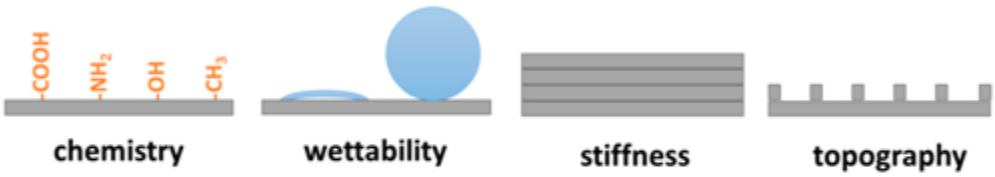

Figure 2: Surface chemistry, wettability, stiffness and topography of biomaterials can all effectively affect the physical adhesion process of cells.

The main target of tissue-engineered scaffolds in regenerative medicine is to mimic the features of ECM and the surrounding environment in order to promote and speed up reparative process. Like ECM, biomimetic scaffolds should allow cell attachment and migration, enable diffusion of vital cell nutrients and wastes, and retain cells. Moreover, the scaffold mechanical properties should be compatible with tissue at implant site so that the new tissue can form and operate normally.[12] The development of biomaterial substrates with the requisite cues to stimulate cells to respond in a predictable way would have exciting implications for tissue engineering and the control of the multipotent capability of stem cells.[13]

Ideally, a suitable scaffold should be a biomaterial device with biological, physical, chemical and mechanical properties that match those of the target tissue. More specifically, they need to be: (a) biocompatible, with a negligible immune reaction, (b) porous, with highly interconnected structure to ensure adequate diffusion of nutrients to cells, gas exchange (i.e.,O_2 and CO_2) and metabolic waste removal, (c) mechanically stable, to provide structural support

to cells and (d) biodegradable, with a degradation rate in synchrony with defect healing rate.[14,15]

Biomaterials can be defined as being natural or synthetic, capable of being tolerated permanently or temporarily by the human body.[6] Polymeric materials provide a broad range of structural properties and offer numerous benefits as biomaterials and that's why they have been utilized in medical implants for nearly 80 years. Polymethylmethacrylate (PMMA) was first used in the body in the 1930s and was initially chosen for its biocompatibility, stiffness, and optical properties. One primary advantage of polymeric materials is that their macromolecular structure provides many biomimetic properties that can be utilized in the body. The elastic modulus and strength of a polymer can be tailored through chemistry and processing to provide values that are bounded by those of biological materials.[16]

1.2.1 Naturally derived biomaterials

Natural biomaterials present a crucial subset of biomaterials for use as tissue engineering templates due to their bioactivity, biocompatibility, tunable degradation, mechanical kinetics and their structural resemblance of native tissue ECM. They are often processed using environmentally–friendly aqueous-based methods. Upon application within biological systems, they do not release cytotoxic products during degradation. An advantage of natural biomaterials is their innate ability to promote biological recognition, which may positively support cell adhesion and function.

Naturally derived biomaterials may typically be divided into two groups: *protein-based biomaterials*, such as collagen, silk fibroin, gelatin, fibronectin, keratin, fibrin and eggshell membrane and *polysaccharide-based biomaterials*, such as hyaluronan, cellulose, glucose, alginate, chondroitin, and chitin. Protein-based biomaterials are typically obtained from animal and human sources and include bioactive molecules that mimic the extracellular environment, whereas polysaccharide-based biomaterials are mostly obtained from algae or from microbial sources. Due to the key advantage of these materials in supporting the attachment, proliferation and differentiation of cells, natural polymers have been extensively explored in the development of tissue engineering templates, often in combination with molecular and mechanical signals, for applications ranging from tissue repair to functional organ replacement.

The main disadvantages of naturally derived biomaterials include the difficulty of isolating them from living organisms and the complicated stages required for their proper preparation, their weak mechanical strength and low structural integrity. To overcome these limitations, recent advances in tissue engineering template redesign have led to the development of biomimetic scaffolds that incorporate ligands imitating the native ECM.[4]

1.2.2 Synthetic polymer biomaterials

The use of synthetic polymers as matrices in tissue engineering presents several key advantages relative to naturally derived polymers, offering attractive options for the control of shape, architecture and chemistry to generate reasonable mimics of ECM systems of human origin. The most widely used synthetic polymers for tissue regeneration are poly(α-hydroxy acids), which include polylactic acid (PLA), polyglycolic acid (PGA) and their copolymer, poly(lactic-co-glycolic acid) (PLGA). Due to its exceptional qualities, such as its biocompatibility, low immunogenicity, hydrolysis under physiological conditions and FDA approval for clinical use, polycaprolactone (PCL) is another synthetic polyester based on hydroxyalkanoic acids that has attracted intense attention in tissue engineering. This polymer is used either alone, as hydrophobic PCL, or in combination with other agents. The properties of synthetic polymers, such as tensile strength, the mechanical modulus and the degradation rate, can be easily tailored for target applications by altering the polymerization parameters. To prepare stronger, mechanically stable and easy to engineer scaffolds, synthetic biomaterials are often preferred.

Although synthetic polymers themselves typically do not carry a risk of inducing an immune response because of a lack of biologically functional domains, certain classes such as poly (α-hydroxy esters), may produce acidic degradation products that can alter the pH of their surrounding tissues. In turn, this pH change can affect cell behavior and survival and cause adverse tissue and inflammatory reactions. The fact of lack functional domains is also a limitation because the lack of peptide side-chain reactivity for binding regulatory peptides, growth factors and other biological signals does not allow the facilitation of cell adhesion or direct phenotypic expression, as a natural polymer would. However, various synthesis techniques have been developed and optimized to incorporate biologically active domains into synthetic polymer templates, thereby enabling the production of biomimetic scaffolds with a defined and tunable composition.[17]

1.2.3 Polycaprolactone (PCL) scaffolds

The production and optimization of different types of scaffolds has been the subject of interest for applications in the repair of various body tissues such as bone in recent years. The design and selection of a biomaterial is a critical step in the development of scaffolds for tissue engineering. The ideal biomaterial should be non-toxic, biocompatible, promoting favorable cellular interactions and tissue development, while possessing excellent mechanical and physical properties. Scaffold should hold mechanical strength to combat the physiological stress occurring at the site of implantation, and it should be in coherence with the mechanical properties of target tissue. Further, it should be able to support the tissue until it is capable of supporting itself. In addition, it

could be biodegradable and bioresorbable to support the reconstruction of a new tissue without inflammation.[14]

In the present study, we chose to fabricate scaffolds using polycaprolactone (PCL) by soft-lithography method. Polycaprolactone (PCL) is a linear synthetic biodegradable aliphatic polyester with semicrystalline structure (Fig.3). It is a polymer having melting point ranging between 59 and 64°C, but its glass transition temperature is about – 60 °C. At room temperature, PCL is soluble in most of the organic solvents at various extents. For instance, it is highly soluble in chloroform, dichloromethane, carbon tetrachloride, benzene, toluene, cyclohexanone and 2-nitropropane, whereas alcohols, petroleum ether, diethyl ether and water cannot dissolve PCL.[18] It has been widely used in various biomedical fields, including drug delivery systems, scaffolds in tissue engineering and sutures, due to its good biodegradability, easy processing, non-toxicity, biocompatibility and good mechanical properties.[19]

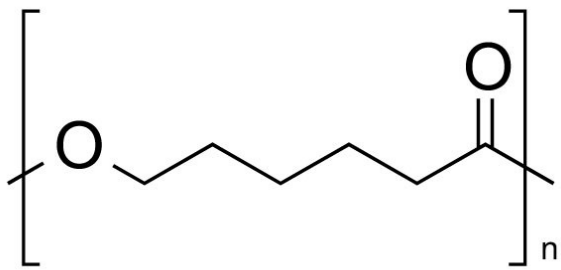

Figure 3: Chemical structure of polycaprolactone

PCL is relatively cheap, and its ability to mold into different forms makes it different from the other biomaterials used in scaffold development.[18] It possess an excellent thermal stability, and most importantly, it is FDA-approved polyester making it fit for tissue engineering applications. Hence, it is susceptible to surface modifications since its properties can be greatly altered. Latest advances in tissue engineering have led to the development of scaffolds with ideal properties by using composites or blends of PCL.

Despite of all the aforementioned characteristics, PCL has two notable limitations. At first, PCL is a hydrophobic material which is a significant barrier to cell attachment and proliferation and, secondarily, it has low degradation rate compare to other polymers, like polylactic acid (PLA) and poly glycolic acid (PGA). PCL is degraded by hydrolysis of its ester linkages under basal conditions. It has been reported that it took 3 years for PCL with a molecular weight of 50,000 to be completely removed from the host body.[6]

To overcome these problems, surface modification and blending with a variety of biopolymers are proved to be a successful approach. Ability of blending with other polymers or ceramics, to enable the alteration of properties according the required application, is one of the rare and most advantageous aspects of PCL polymer which makes it popular choice as scaffold fabrication material (Fig.4). In the field of surface modifications, the most commonly used methods are the

surface coating, with proteins or other bioactive molecules, and plasma etching.[20,21]

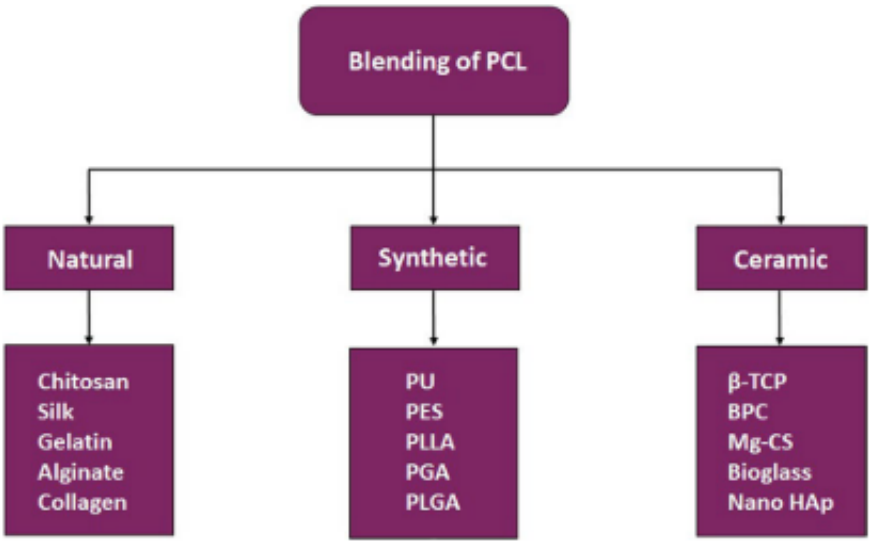

Figure 4: Natural, synthetic and ceramic polymers which are usually blending with PCL [18]

1.2.4 Tailor made biomaterials with specific topographical characteristics

Cells *in vivo* are exposed to a broad variety of physical cues depending on their functions and locations. Many studies have shown that soluble factors such as growth factors, hormones and small molecules can induce stem cells differentiation; however, some of the differentiating pathways can be activated regardless of these factors.[22] The biophysical properties of extracellular matrix, e.g., topography, stiffness, elasticity and bioelectricity have influence on the behavior of stem cells.[23,24,25] Cells convert physical stimuli into biochemical signals through mechanotransductive processes.[26]

In this sense, the need arises for the design of biomaterials with architectures that mimic the natural environments of cells. While the role of biochemical signals is well-documented, the importance of biophysical cues has received more recognition and attention only in the last decade. Current advances in microfabrication technologies have enabled the generation of substrates with nano/micro-scale topographies to study the effects of biophysical signals on cellular function.[27]

Among the biomaterial properties that affect cell behavior, surface topography has shown an enormous potential to control cell morphology, spreading and orientation through a phenomenon known as contact guidance[23]. Contact guidance is defined as the elongation or morphological alteration of a cell in response to physical cues.[16] Topographical features of varying size, shape and

spacing can determine cell attachment, integrin clustering, cytoskeletal structure, cell shape and cell polarity altering their mechanotransductive signaling and in turn downstream behaviors including differentiation.[28,29]

The cytoskeletal-generated force exerted by the surface properties of the adhering substrates are transmitted into nucleus to induce adaptive cellular functional changes.[30,31] Surface modifications offer a simple and cost-effective alternative to traditional differentiation techniques that would otherwise require growth factors or other biochemicals that are relatively unstable and expensive.[26]

Several researches have revealed that micro- and nano-scale topographies (Fig.5) in the form of pillars, grooves, pits, or ridges can induce the differentiation of human mesenchymal stem cells (MSCs) to a certain cell lineage.[32,33] Cells can "sense" substrate elasticity and surface patterns ranging from 10 nm to 100 mm.[34] This recognition is particularly mediated by *integrin receptors*, which operate as the main transducers of mechanical stimuli across cell membrane by linking ECM and the cytoskeletal, and in combination with several other proteins like vinculin form focal adhesions.[30] Topographic influence of cells to micrometer range features was reported by Curtis in 1964 and has since been extensively studied and well-established.[35]

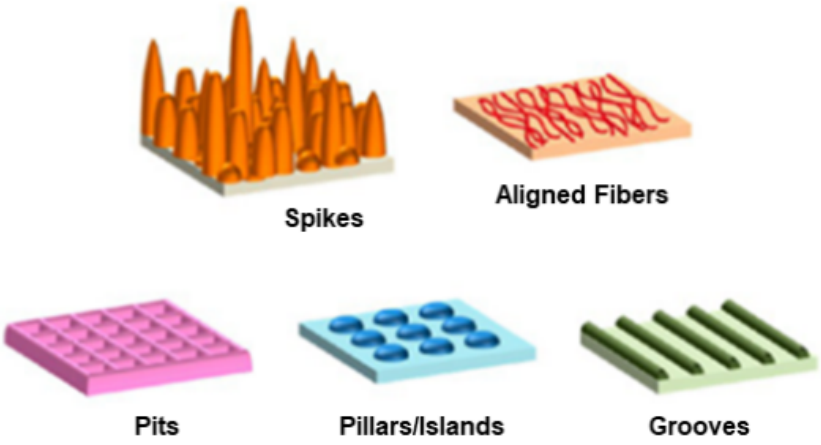

Figure 5: Patterned surface topographies that affect cell behavior[36]

1.2.5 Cell adhesion onto biomaterials' surfaces

The basic concept underlying TE involves the combination of scaffolds with living cells and bioactive molecules to produce a tissue-engineering construct, which is subsequently implanted into the defect site promoting tissue regeneration. Scaffolds must present a good interaction with both seeded and surrounding cells, which is fundamental to stimulate the ECM synthesis and the tissue regeneration process.[37]

Cell adhesion is the ability to attach to another cell or to the ECM by transmitting extracellular or intracellular forces. It plays a critical role in cells communication, stimulation of signals regulating cells differentiation, cell cycles, migration and survival. ECM provides biological information, which are coded by proteoglycans, glycosaminoglycans (GAGs) and alternative soluble molecules, for instance growth factors as well as cytokines.

Cell-matrix (scaffold) anchorage is formed by *integrins* (transmembrane proteins)[38], whereas cell-cell adhesion is formed by *adhesion molecules*. Both the integrins and adhesion molecules are attached to the tensile members of the cytoskeleton, the actin filaments, through the focal adhesion (FA) complex, a highly organized cluster of molecules.[39] The cytoskeletal structure holds the nucleus and maintains the shape of the cell. Integrins recognize and translate surface signals into the indicated response, mediate adhesion to a physical surface to establish cellular orientation and spatial organization.

The process of static *in vitro* cell adhesion is characterized by three stages (Fig.6): attachment of the cell body to its substrate by electrostatic forces (phase I), flattening by integrin bonding (phase II), spreading of the cell body and organization of the actin skeleton with the formation of focal adhesion between the cell and its substrate (phase III). The spreading process is the combination of continuing adhesion with the reorganization and distribution of the actin skeleton around the cell's body edge. The strength of adhesion becomes stronger with the length of time a cell is allowed to adhere to a substrate or another cell.[40]

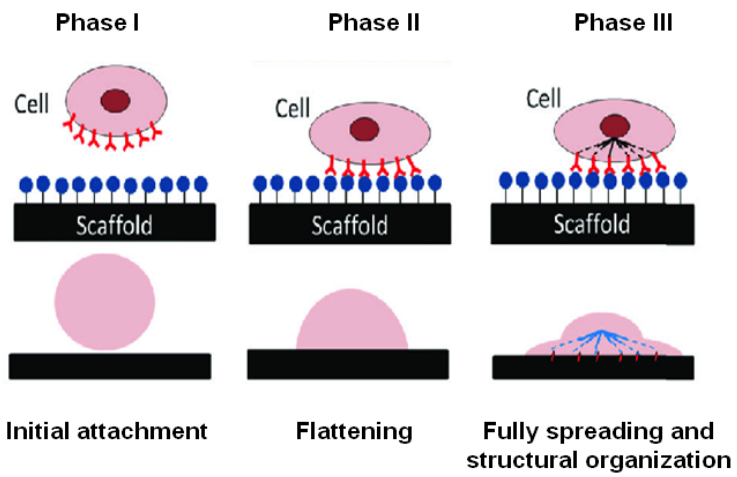

Figure 6: Schematic of the phases of passive in vitro cell adhesion. Phase I: sedimentation of cells can be enhanced through electrostatic interactions, Phase II: cell attachment is facilitated through the formation of integrin binding sites between the cell and scaffold and Phase III: cell spreading occurs through focal adhesions[39]

Cell-material adhesion is a complex, multifactorial process and can be either *specific*, with cell receptor recognition or binding to proteins or peptides or *nonspecific*, by non-covalent attractive forces between cells and the biomaterial. Surface properties of biomaterials have the ability to guide complex

processes of cell adhesion. Tailor made surfaces for controlling cell–material interactions is an interesting subject in the field of implantable medical devices and engineered tissues. Using different approaches, various materials have been surface engineered in order to guide cell adhesion and modulate cell–biomaterial interactions, indicating that cell growth, division and migration are highly dependent on their immediate culture substrate. Studies have highlighted the importance of surface properties such as *roughness*[41,8], *topography*[42], *chemistry*[43,44], *wettability*[45] and *energy* in the modulation of cell proliferation and differentiation.

1.2.6 Effect of scaffolds' wettability on cell adhesion

Surface wetting is determined by the balance between adhesive and cohesive forces and it depends on the value of contact angle, measured on the droplet deposited on the substrate (solid surface), at the contact point of solid, liquid and gas phases.[39] Materials can be considered as *hydrophobic*, displaying water contact angles above 90° and *hydrophilic*, if the water contact angle is smaller than 90°, with greater contact angle hysteresis.[46] It is widely accepted that biomaterial surfaces affect protein adsorption and the subsequent activation of cells. Surface wettability plays an important role in regulating cell behaviors, which has been extensively studied.

Each type of cell has its own unique characteristics including how cells actually respond to different surfaces. This may explain the fact that superhydrophobic surfaces were reported to be extremely cell repellent in some works[47,48], however, in other works, it was demonstrated that cells not only adhere but also proliferate on superhydrophobic surfaces.[49]

Cell adhesion is mediated by cell membrane proteins. Proteins are amphoteric molecules carrying charges depending on surrounding pH. Thus, proteins are positively charged when the pH values are below their isoelectric point (Ip) and negatively charged when pH values are above their Ip. Positively charged surfaces enhance adsorption of proteins with Ip below 5.5, whereas negatively charged surfaces increase adsorption of proteins with Ip above it. Surface charge determines the amount, type and refolding degree of absorbed proteins and so, affects cell adhesion. The surface charge can render the surface into more hydrophilic and is extremely important in the initial stages of cell attachment as it controls the formation of focal adhesion with biomaterial's surface.

Many factors such as ions adsorption, plasma treatment protonation/deprotonation, dissociation of surface chemical groups and application of the external electric field may cause charging of materials surface and therefore change of the surface free energy, which is a thermodynamic quantity describing the equilibrium state of atoms on the surface of the

materials.[39] The surface free energy and the wettability of surfaces are directly related concepts.

Apart from chemical treatment methods, a very common way to change wettability of surfaces is by tuning the surface roughness. Roughness typically increases the water contact angle (CA), so enhances hydrophobicity. Some studies showed that nano- and micro-topography and, in particular roughness, increase cell adhesion[50,51] but other revealed the opposite behavior.[52,53] So, the details of surface topography may exert both positive and negative influences on cell adhesion and spreading and the observed effect is extremely dependent not only on the properties of the surface but also on the cell type.[48]

1.3 Soft lithography

Microfabrication has become important to biology in order to fabricate cell culture scaffolds to mimic the natural extracellular environment features. There are many micro-patterning techniques that can be used to produce designing surfaces and ordered structures, such as grooves, pits, pillars, spikes and wells with nano- to micrometer scale, on biomaterials surfaces, which could simulate the microenvironment of cell growth and tissue regeneration.[54]

Over the past two decades, soft lithography, as one of the most important micropatterning techniques, known for its non-toxicity and easy operation, has attracted more and more attention in tissue engineering, because it could fabricate precise topographical features of natural or synthetic biopolymers by printing, molding, or embossing using an elastomer with a patterned surface as a mask, stamp or mold.[19,55] Soft lithography represents a different approach to rapid prototyping of various types of both microscale and nanoscale structures on planar, curved, flexible and soft substrates especially when low cost is required. It has been successfully used to transfer well-defined microsized patterns from silicon or stainless-steel masters to surfaces of soft biomaterials, allowing the replication of controlled microenvironments and in-depth study of the influence of surface properties on cell behavior.[54]

An elastomeric stamp, mold, or mask having specific structures on its surface is the key element of soft lithography.[56] It is usually prepared by replica molding by casting the liquid prepolymer of an elastomer against a master that has a patterned relief structure in its surface. Because masters are typically rigid, the use of an elastomer facilitates separation of master and replica. The mechanical properties of an elastomeric stamp are critical to its ability to transfer a pattern with high fidelity. Poly(dimethylsiloxane) (PDMS) is the most widely used material for making elastomeric molds due to its outstanding properties, such as excellent flexibility, durability, chemical resistance, reversible deforming without permanent deformation of the surface topography, optical transparency and low cost.[57,56] PDMS also has a low surface free energy (21.6 dynes/cm^2), and reversibly conforms to different surfaces, even nonplanar

structures.[58] It has a shear modulus of 0.25 MPa and a Young's modulus of roughly 0.5 MPa (characteristic of a moderately stiff elastomer). This elastomeric character allows it to conform to a surface and achieve atomic-level contact.[59] Also, the elastic characteristic of PDMS allows it to be released easily, even from complex and fragile structures. An elastomeric mold also offers the opportunity to manipulate the size and shape of features present on the mold by mechanical deformation. Furthermore, PDMS is a durable elastomer and it can be used up to about 100 times without noticeable degradation in performance.[60]

A large number of patterning techniques form the basis of soft lithography. These are: microcontact printing (μCP), replica molding (REM), microtransfer molding (mTM), micromolding in capillary (MIMIC), solvent-assisted micromolding (SAMIM), phase-shifting edge lithography, nanotransfer printing, decal transfer lithography and nanoskiving.[59] These techniques are called as "soft lithography" because in each case an elastomeric stamp or mold is the key element that transfers the pattern to the substrate and, more broadly, because each uses flexible organic molecules and materials.

In this scientific study, replica molding (REM) technique was used for the fabrication of PDMS molds and, after that, for the preparation of polycaprolactone (PCL) replicas. Generally, REM consists of three steps: (i) creating a topographically patterned master (ii) transferring this pattern to PDMS by curing a PDMS prepolymer in contact with the master and releasing the PDMS from the master and (iii) transferring the pattern on the PDMS back into a replica of the original master by solidifying a liquid prepolymer against the PDMS mold and releasing the solidified structure to isolate a replica of the master (Fig.7).[58,59] Examples of these solidified structures include polymers, gels, precursors to ceramics and carbons, luminescent phosphors, salts, and colloids. The PDMS mold releases easily from both the original master and the replica without damage to either surface. Repeating the replication procedure can pattern numerous molds from each master and multiple replicas from each mold. The process replicates structures with high fidelity and accuracy down to length scales similar to the size of large molecules.

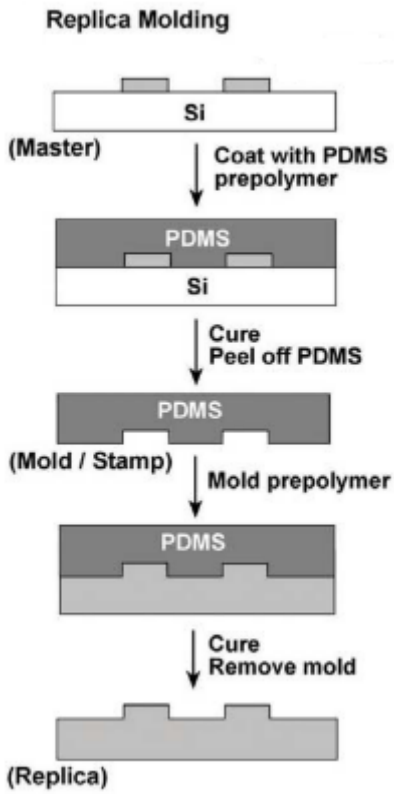

Figure 7: Schematic illustration of the procedure to form elastomeric molds from topographically patterned masters, and molding of this elastomer with another prepolymer to fabricate a replica of the original master. [58]

1.4 Mesenchymal stem cells (MSCs)

Stem cells are unspecialized cells that have the remarkable potential to differentiate into many cell types during embryo development and growth. Under certain physiological or experimental conditions, stem cells can be induced to become tissue or organ-specific cells having special functions, thus offer a source of precursor cells for treatment of degenerative, malignant and genetic diseases.[22] A type of adult stem cells, the multipotent mesenchymal stem cells (MSCs) have been extensively studied for over three decades for their therapeutic potential over a wide range of diseases. The biological history of adult stem cells dates back to 1909 with the discovery of Hematopoietic stem cells (HSCs) in bone marrow.[61] In 1970, Alexander Friedenstein and colleagues derived bone marrow and spleen cells from guinea-pig and discovered that MSCs are capable of forming tremendous fibroblast colonies.[62] They referred to a unique bone marrow cell population with characteristics of plastic adherence and multi lineage differentiation capacity as colony forming unit fibroblasts (CFU-F).[63] In the early 1990s, CFU-F generated global interest in science and clinical practice, and became popularly known as “Mesenchymal Stem Cells (MSCs)”.[64]

MSCs have a characteristic spindle shaped morphology (Fig.8) and they are capable of self-renewing and differentiating into several lineages including adipocytes, osteocytes and chondrocytes.[65] They have been isolated from various tissues and organs including bone marrow, adipose tissue, placenta, umbilical cord blood, the testes, the liver, the pancreas, the spleen, amniotic fluid, menstrual blood, dental pulp, the dermis and the lung.[66] The source can be either human (adult or embryo) or animal origin.[62] They possess cellular integrity with low variability from different adult donors. They show differential morphology, growth rate, proliferation and differentiation potential, transcriptomic/proteomic signature depending on their source of origin and biophysical cues such as cell culture media, fetal bovine serum, growth factors, as well as surface topography and kinds of extracellular matrix used during the culture.[67] Since their easily isolation from different tissues and, due to their rapid proliferation, multipotency and their unique immunomodulatory properties they have been using as ideal cells for tissue engineering and regenerative medicine therapies.[68]

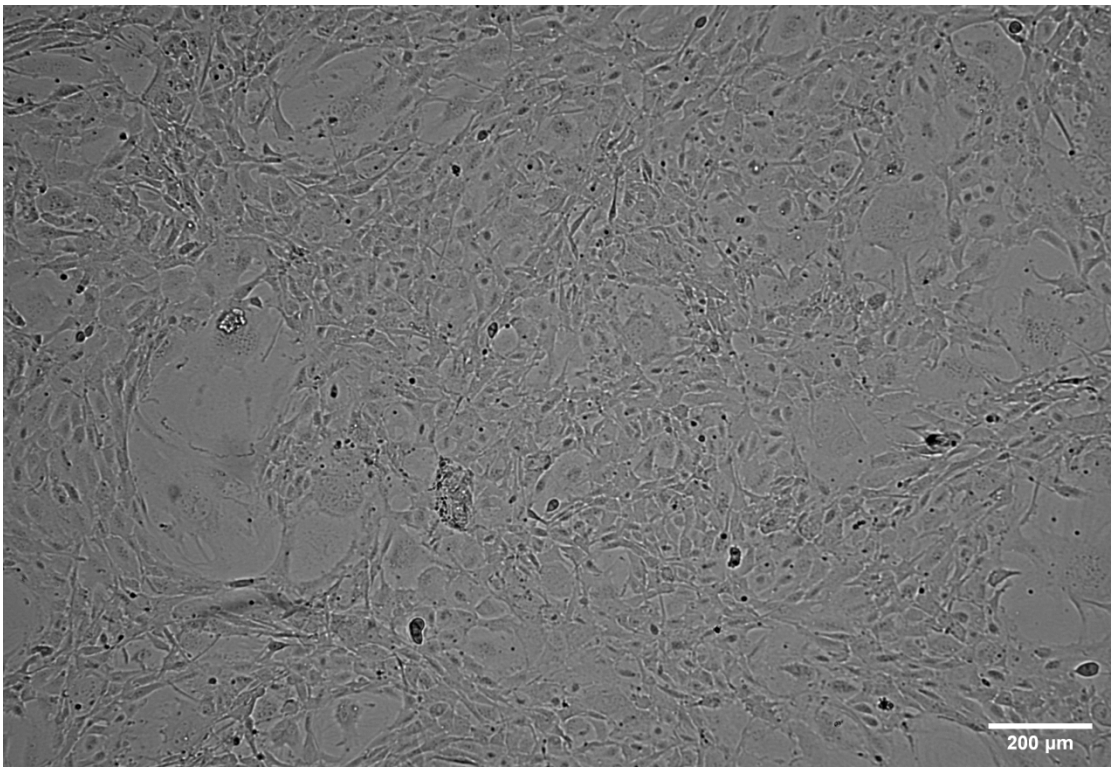

Figure 8: MSCs (passage 8) as they are growing in cell culture flask. Picture was taken with optical microscope (Nikon Eclipse Ts2k inverted microscope).

1.5 Osteogenic differentiation of Mesenchymal stem cells (MSCs)

Bone defects are a major health concern around the world due to the damage of bone tissue either by injuries (sport-related, motor accident) or various diseases such as osteoporosis, arthritis, neoplasm, and congenital

malformations which some of them are related to ageing.[69] Unlike other tissues, bone can regenerate itself and in most cases, bone injuries heal without scar formation, as is the case, for example, with fractured bones. Even so, bone is one of the most frequently transplanted tissues.[70] Due to organ donor shortage and the problems associated with allograph transplantation, bone tissue engineering has emerged as a promising alternative for bone implantation to repair or replace the diseased bones.[71] The last two decades, a great deal of efforts has focused in the field of bone tissue engineering, and, particularly, in the area of stem cells, such as MSCs because of their potential to differentiate into various cell lineages, and how to modulate their behavior through environmental cues.[72]

Osteogenic differentiation of MSCs *in vitro* largely depends on the culture conditions and, specifically, it is induced by the presence of dexamethasone, ascorbic acid and β-glycerol phosphate.[73] The speed and efficacy of cells differentiating into mature osteoblasts and their lifespan determines the rate of bone formation. The osteogenic differentiation of MSCs in vitro has been divided into three stages. These processes are mediated by osteoblasts, which work in tight cooperation with osteoclasts, together constituting a "bone multicellular unit". The osteoblasts synthesize the bone extracellular matrix and the osteoclasts carve out the shape to fit the physical environment and adjust it to the demands of the body growth. Fine tuning of this system is crucial for the development of bones, for repairing fractures, and for the correct maintenance of the skeleton throughout life.[74] Thus, the first stage consists of days one to four where a peak in the number of cells is seen. This is followed by early cell differentiation from days 5 to 14, which is characterized by the transcription and protein expression of alkaline phosphatase (ALP). After this initial peak of ALP its level starts to decline. The final stage from days 14 to 28 results in a high expression of osteocalcin and osteopontin, followed by calcium and phosphate deposition.[75] At this stage the osteoblast assumes its characteristic cuboidal shape (Fig.9).[74]

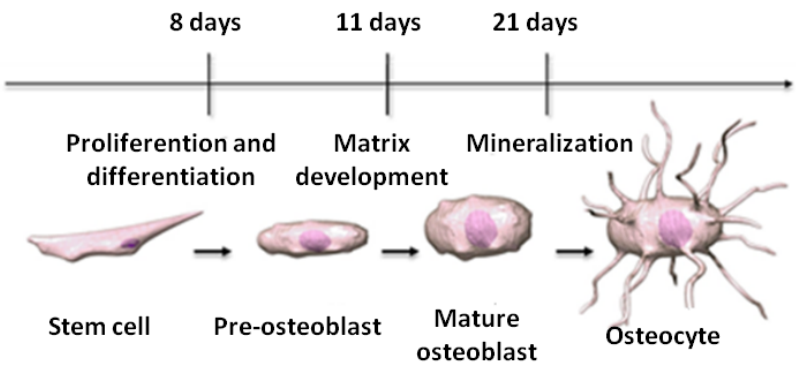

Figure 9: Schematic illustration of stem cells differentiation towards osteocytes[72]

The detection and evaluation of the degree of osteogenic differentiation is quite important in orthopedic and related diseases. During osteogenic differentiation, collagen-enriched extracellular matrix is formed, and calcium ions (Ca^{2+}) and inorganic phosphate accumulate to form hydroxyapatite crystals. Matrix mineralization in cell cultures is the most important indicator of osteogenic differentiation. Many biochemical analysis methods such as immunostaining, quantitative real-time polymerase chain reaction (RT-qPCR) and protein blotting assays have been developed to observe the degree of osteogenic differentiation in clinic and scientific research. Among these strategies, the quantification of mineralization based on Alizarin Red-S staining is the most common method. Given to the high sensitivity and easy operation, fluorescent probes have also been developed for the detection of biomarkers, such as alkaline phosphatase (ALP), to detect the osteogenic differentiation.[76] In this work, we evaluated MSCs osteogenic differentiation with both Alizarin Red-S staining and ALP activity.

2. Materials and Methods

2.1 Physicochemical studies of polycaprolactone scaffolds

2.1.1 Fabrication of laser micro-structured substrates and PDMS negative molds

Single-crystal n-type silicon (1 0 0) wafers were subjected to laser irradiation in a vacuum chamber evacuated down to a residual pressure of 10^{-2} mbar. A Yb:KGW laser was used with a pulse duration equal to 170 fs, 1 kHz repetition rate, and 1026 nm wavelength. The laser fluences used were 0.25 J/cm^2 and 0.66 J/cm^2, thus creating two different topographies, defined as low and high roughness, respectively. The overall spike area was 0.5 cm × 0.5 cm. The laser-fabricated Si substrate is characterized as the “master” substrate.

Negative replicas of the two categories master Si substrates were produced on elastomeric PDMS. In particular, liquid PDMS was poured onto each substrate. Then, the PDMS-coated Si substrates were placed into a vacuum chamber to remove residual air bubbles, thus providing for better penetration of the polymer into the laser microstructures. After heating at 80 ˚C for 2 h, a mold, which holds the negative of the original pattern, was peeled off of each Si substrate. An adequate number of PDMS negative molds were produced for each group (low and high roughness topographies). In this master thesis defense, the Si substrates and the PDMS negative molds were fabricated once by two members of the group (Despina Angelaki and Paraskevi Kavatzikidou, respectively) and they were used for the reproduction of the initial Si morphologies by producing PCL replicas.

2.1.2 Fabrication of polycaprolactone replicas

Using the PDMS negative mold (negative spikes morphology), we succeeded the reproduction of the initial Si morphologies by producing PCL replicas. A PCL (Mw=80kDa) polymeric solution of 8% in chloroform /methanol (4/1) was carefully prepared, by magnetically stirring for 2 h at room temperature (RT). One droplet of the PCL solution was poured onto each PDMS negative mold. Following the evaporation of the solvents (chloroform in 61.2°C and methanol in 64.7°C), the PCL-coated PDMS mold was heated on a heating plate in 65°C for 90min. Then, the PCL replica was peeled from the PDMS negative mold with a pair of tweezers.

2.2.3 Water contact angle measurements

The contact angles of the patterned and flat PCL substrates were calculated via an automated tensiometer (DataPhysics OCA – Series), using the sessile drop method. A droplet of distilled, deionized millipore water with a volume of 1 μL was positioned on the surface of the substrates using a microsyringe and images were taken with an integrated camera. The contact angle values formed at the liquid–solid interface were calculated automatically by the software (SCA-20).

2.2 Cell studies

2.2.1 Cell cultures

For all cell cultures at this study, Mesenchymal Stem Cells (MSCs) C57BL/6 from mice bone marrow was used. MSCs were grown in cell culture flasks using Dulbecco's modified Eagle's medium (DMEM) – low glucose (1000mgr/L glucose) supplemented with 10% fetal bovine serum (FBS) and 1% penicillin/streptomycin solution (PS) at 37°C in a 5% CO_2 incubator, with medium renewal every 3-4 days. MSCs used for the experiments have a passage ranging from 5-10. PCL substrates were UV sterilized and transferred into sterile wells of 24-well plates. Then, 3×10^4 or 5×10^4 cells per ml (depending on the needs of the different experiments) in culture medium were seeded on the PCL substrates and were cultured for a series of different time periods. The control samples in all the experiments were tissue culture plastic (TCP) coverslips (polystyrene).

2.2.2 Scanning electron microscopy biological samples preparation-dehydration procedure

The morphology of MSCs growing on the patterned PCL surfaces was analyzed by SEM (Jeol JSM – 639 OLV). After culture termination, the cells were fixed following a specific fixation protocol. The medium was removed from samples and they were washed twice with PBS (pH = 7.4) for 10 min. Then they were fixed with 2% glutaraldehyde (GDA) in SCB/H_2O (1:1) fixative buffer for 30 min at 4°C. After the end of 30 min, samples were washed twice (for 10 min each

time) with SCB at 4°C. The samples at dehydration phase were washed in graded series of 30%, 50%, 70%, 90%, and 100% EtOH for 7 min each at 4°C. Then, the samples immersed in hexamethyldisilizane (HDMS)/ EtOH (50:50) solution for 30 min twice and, finally, in 100% HDMS for 20 min twice at RT. As a final step, HDMS removed and samples left to dry completely overnight. Prior to electron microscopy examination, the samples were sputter-coated with a 15nm film of Au (BAL-TEC SCD 050).

2.2.3 Live/Dead Assay

A LIVE/DEAD™ Viability/Cytotoxicity Assay Kit for mammalian cells was used for evaluating cell viability and proliferation. For this purpose, MSCs were seeded onto PCL replicas to a density of 3×10^4 cells/ml. After 3 and 10 days of incubation under standardized culture conditions as described above, medium was removed and cells on PCL replicas were washed twice with PBS. A live/dead solution was prepared by adding 20 μL of the supplied 2 mM ethidium homodimer-1 (EthD-1) stock solution to 10 mL of sterile PBS (thus reaching the desired concentration of 4 μM EthD-1 solution) and, after mixing, 5 μL of the supplied 4 mM calcein AM stock solution was added to the 10 mL EthD-1 solution (thus reaching the desired concentration of 2 μM calcein AM solution). The live/dead solution with the volume of 500μl was directly added to the samples in order to cover the whole replicas and was left for 45 min at RT. Finally, the cells were washed once with PBS, and fluorescent images were obtained by confocal microscope (Leica SP8 inverted Confocal Microscope).

2.2.4 Osteogenic differentiation

To induce osteogenic differentiation, three days after MSCs culturing as described above, the standard culture medium removed and the osteogenic medium added which consisted of DMEM - high glucose (4500mgr/L glucose), 10% FBS, 1% penicillin/streptomycin, 0.1 mM dexamethasone, 0.17mM L-ascorbic acid and 10 mM β-glycerophosphate. The osteogenic medium was renewed every three days in order to observe MSCs differentiation.

2.2.5 Immunocytochemical assay

For this assay, the medium was removed from samples and they were washed twice with PBS (pH = 7.4) for 5 min and then fixed with 4% paraformaldehyde (PFA) for 15 min at RT. After removal of PFA solution, the samples were washed again with a PBS solution and treated with Triton-X100 0.1% solution in PBS for 5 min in order to permeabilize cell membranes. Then, the samples were washed with PBS solution for 5 min and blocked using 2% BSA in PBS solution for 30 min. Subsequently, the cells incubated with the first antibody overnight at 4°C. Next day, the cultured cells washed with PBS and incubated with the secondary antibody and actin phalloidin for 2 h and then nuclear staining carried out by 4,6-diamidino- 2-phenylindole (DAPI 1:10.000 in PBS) at RT. The first and second antibodies used in the present study are

summarized in Table 1. The samples were transferred on microscope slides for observation using a 'Leica SP8' Confocal Microscope (inverted).

Table 1: The first and second antibodies used for this investigation. Both 1st and 2nd antibodies were diluted in 1% BSA in PBS solution, at the respective concentrations

1st Antibody	2nd Antibody
YAP (1:100)	a-Rabbit 488 (1:300)
CD44(1:100)	a-mouse 568 (1:500)
Vinculin (1:200)	a-mouse 488 or a-mouse 543 (1:500)

2.2.6 Alizarin red S staining

For Alizarin Red S staining, MSCs were seeded on PCL replicas in 24-well plates at a density of 5×10^4 cells/ml and cultured in standard medium, as described above. Three days later, the medium was replaced with osteogenic medium. Alizarin Red S staining was performed at days 21 and 28 after osteogenic differentiation. At each time point, medium was removed from MSCs and the cells washed two times with PBS. Cells were fixed in 4% paraformaldehyde (PFA) for 15 min at room temperature and then washed twice with deionized water. Then, 400μl of 2% solution of Alizarin Red S (pH=4.1-4.3) added at each well and the plate incubated for 1h at RT. After that time, samples washed five times with distilled water to remove any unincorporated ARS. An optical microscope (Leica DM IL Inverted Microscope) with an integrated camera used to inspect the cells and take pictures of red spots that were dyed from ARS. For quantification of matrix mineralization, ARS extracted with a 10% cetylpyridinium chloride (CPC) in 10mM Na_2PO_4 (pH=7.0) solution. Samples with 300μl of CPC solution were incubated for 1h at RT. At last, the supernatant was transferred to a 96-well plate (100μl at each well) and the optical density was measured at 545 nm in a micro-plate Eliza reader.

2.2.7 Alkaline phosphatase activity

ALP activity was quantified using the ALP Assay Kit (Takara). MSCs were seeded on PCL replicas in a 24-well plate at a density of 5×10^4 cells/ml and cultured in standard medium, as described above. Three days later, the medium was replaced with osteogenic medium. ALP activity was quantified at days 14, 21 and 25 after osteogenic differentiation. At each time point, medium was removed from MSCs and the cells washed with physiological saline (0.9 % NaCl). Then, 100μl of the extraction solution (physiological saline including 1 % NP-40) were added to each well for solubilization of suspension and adherent cells. Subsequently, 100μl of the substrate solution [pNPP (p-nitro-phenyl phosphate)] were added to each well. The plate with the extraction and substrate solution was incubated for 1h at 37^0C and after this time the reaction was terminated with 70μl of NaOH 0.5 N. The supernatants were transferred to

a 96-well plate and the optical density was measured at 405 nm in a micro-plate Eliza reader.

2.2.8 Statistical analysis

The data were subjected to one-way ANOVA followed by post hoc Tukey HSD for multiple comparisons between pairs of means. Statistically significant difference between experimental results was indicated by $p < 0.05$.

3. Results and discussion

3.1 Physicochemical study of PCL replicas

3.1.1 Fabrication of polycaprolactone (PCL) replicas

Polycaprolactone (PCL) replicas with three different topographies (flat, low roughness and high roughness) were produced using the method of soft lithography. The micro-structured substrates that used as molds were prepared by ultrafast laser structuring (Fig.10), as described above (chapter 2.1.1)

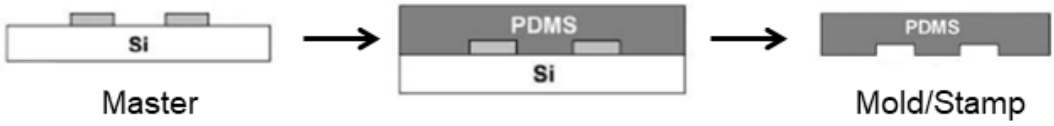

Figure 10: Schematic illustration of the procedure to form PDMS molds from topographically patterned Si masters

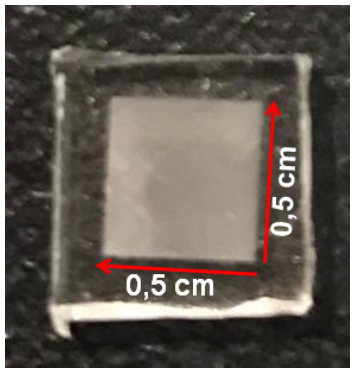

Figure 11: The PDMS negative mold

Using the PDMS negative mold (negative spikes morphology) (Fig.11), replicas of the initial morphology can be made out of PCL (Fig.12). At first, a proper solvent must be found to dissolve the solid PCL (Mw=80kDa) and then poured it onto the PDMS negative molds. According to literature, polycaprolactone is soluble in chloroform, dichloromethane, carbon tetrachloride, benzene, toluene, cyclohexanone and 2-nitropropane.[18] For this assay, we tried to dissolve PCL in dichloromethane and chloroform/methanol 4:1. The last solvent dissolved PCL faster and better than dichloromethane, so *chloroform/methanol 4:1* was preferred as a better solvent for PCL.

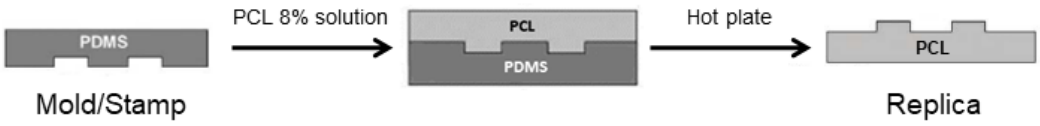

Figure 12: Schematic illustration of the PCL replicas fabrication with PDMS molds

As a second step, PCL solutions with different concentrations were produced in range 6-20% in chloroform /methanol 4:1, in order to clarify which is the ideal PCL concentration to produce replicas. Starting from PCL 6% in chloroform /methanol 4:1, replicas were very thin and were torn when they were peeled from the PDMS negative mold (Fig.13A). PCL concentrations above 10% in chloroform /methanol 4:1 produced replicas full of holes and the solvent evaporated slowly (Fig.13B-D). It was, also, observed that if the solvent has not evaporated completely and the replicas were wet the replication wasn't successful due to the fact that part of the replica remained on the mold when it was peeled off. To solve this problem, a heating plate used to contribute the evaporation of solvent.

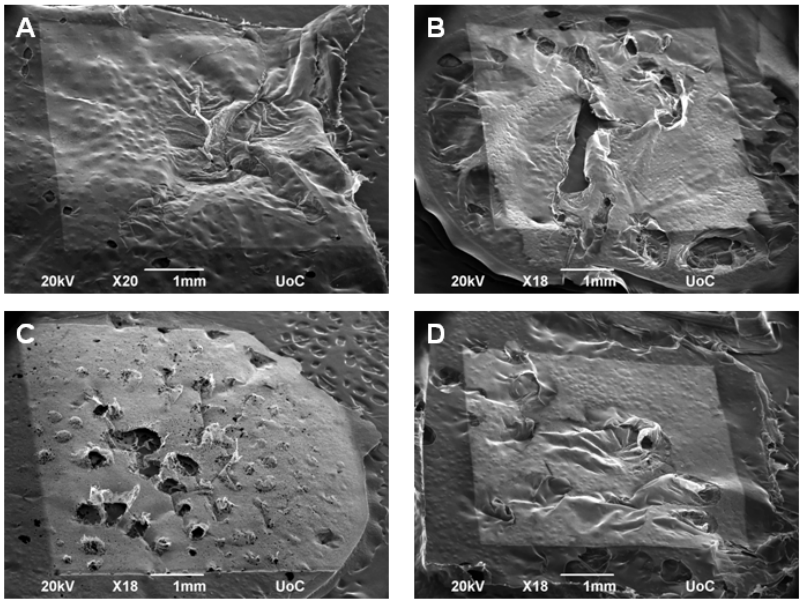

Figure 13: Scanning electron microscopy (SEM) images of: A) 6% B) 10% C) 13% and D) 20% PCL replicas

Considering all the above, it turns out that the appropriate concentration of PCL is from 6% to 10%, because there is a need for a layer of solution not too thin but, also, not too thick. Thus, a PCL 8% solution in chloroform /methanol 4:1 was prepared in order to find the ideal concentration of the polymer to fabricate scaffolds that can be seeded with cells and support cell adhesion, proliferation and differentiation. As it turned out, excellent replicas without damages were produced with the PCL 8% solution as found by SEM images (Fig.14). Moreover, the topographic imprint from the original mold was transferred to the

PCL replicas with great accuracy. The flat PCL replicas were produced by using the PDMS molds from the reverse side, which is free from any topography.

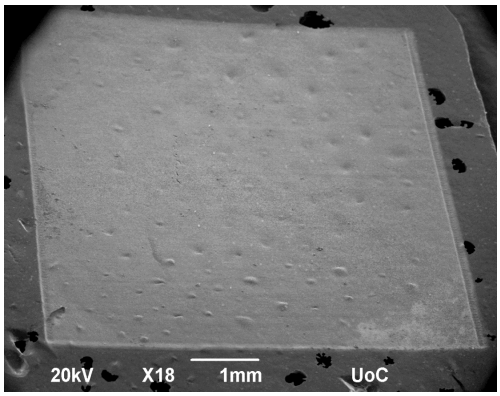

Figure 14: Scanning electron microscopy (SEM) image of PCL 8% replica

3.1.2 Geometrical characterization of PCL replicas with Scanning Electron Microscopy (SEM)

After the successful reproduction of patterned substrates, the surface characteristics of PCL replicas were studied with SEM (Fig.15). The measurements of the geometrical parameters of the spikes on PCL replicas, as calculated from cross section SEM images (Fig.17), are summarized in Table 2 and include the height (h), width (d) and aspect ratio (A). The spikes of low roughness topographies have a height (h) of 2.79±0.1μm and a width (b) of 1.51±0.12 μm. Respectively, the spikes of high roughness topographies have a height (h) of 8.73±1.35μm and a width (b) of 3.23±0.05 μm. The aspect ratio was calculated by dividing the height by the radius of the spike's base (A=h/b). The density of spikes was calculated by top view SEM images using Fiji ImageJ plug-in "Analyze particles" and expressed as the number of spikes per mm^2. While spike density was the lowest in the high roughness structures, the spikes' height, thus aspect ratio, increased. These findings demonstrate the anisotropic nature (aspect ratio≠1) of the PCL substrates. Also, it is obvious from the directionality histograms that there is a varied orientation between the replicas. The high roughness PCL substrate showed a directionality at the area close to zero degrees, while the low roughness substrate showed a lower directionality at the area close to -83 degrees (Fig.16).

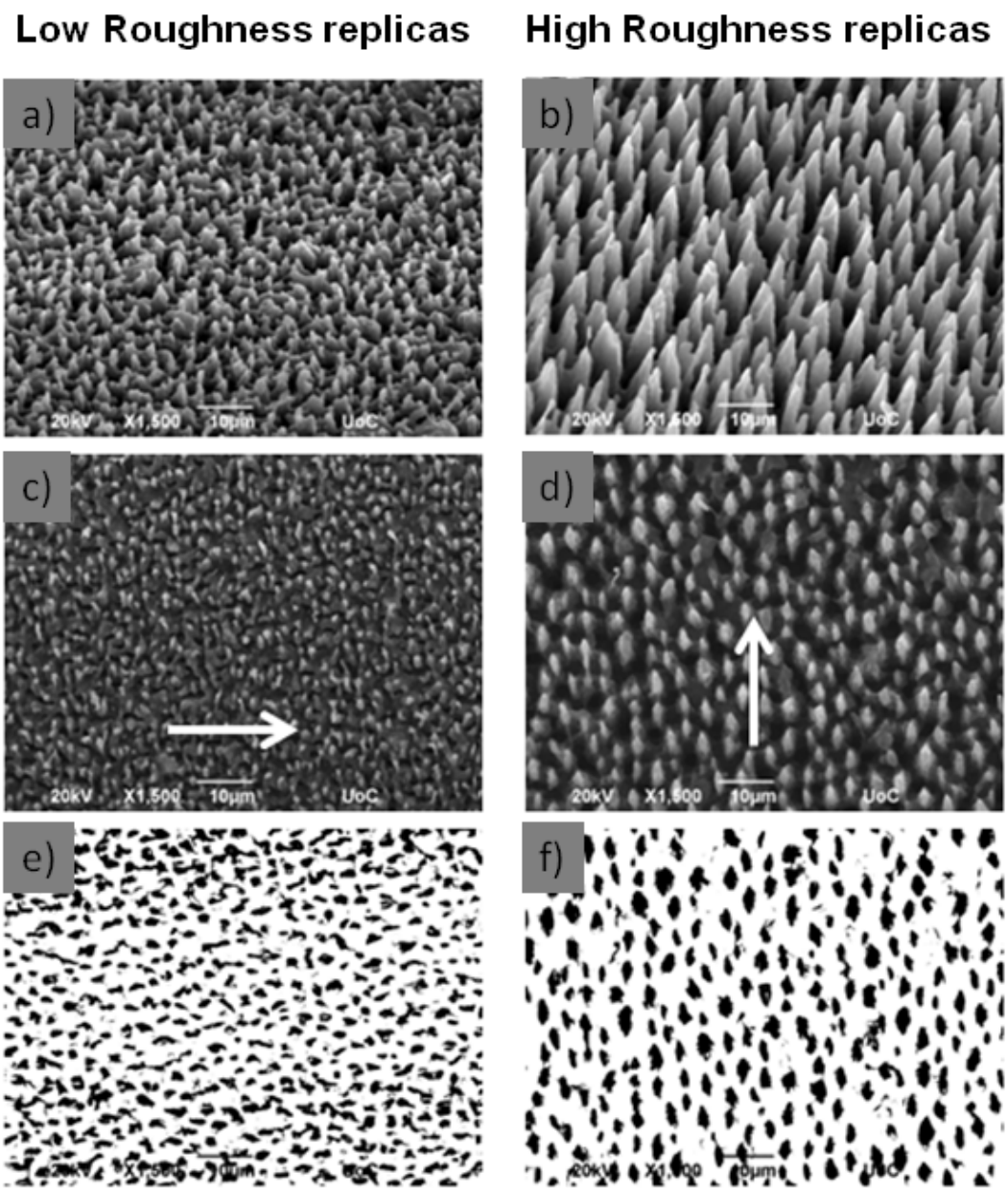

Figure 15: Scanning electron microscopy (SEM) images: tilted (a–b) and top view (c-d) of low roughness and high roughness PCL replicas. The white arrows represent the spikes' direction. The images e-f were generated using the Fiji ImageJ plug-in "Directionality".

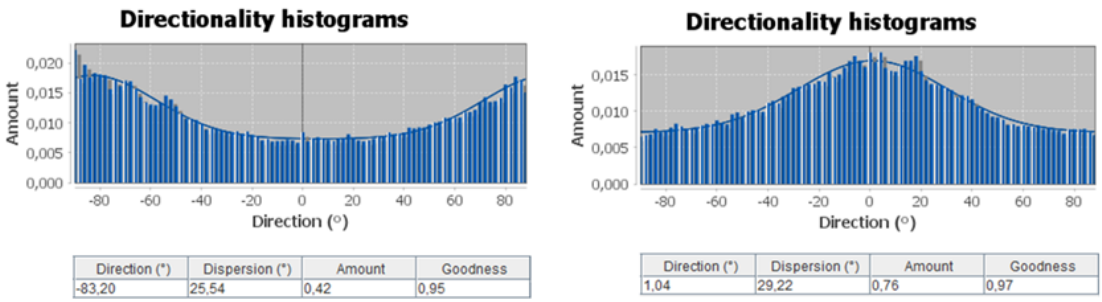

Figure 16: Directionality histograms, which were generated using the Fiji ImageJ plug-in "Directionality". On the left is the histogram for low roughness replicas and on the right is the histogram for high roughness replicas. The plug-in generates statistics for the highest peak found. The highest peak is fitted by a

Gaussian function, taking into account the periodic nature of the histogram. In the tables, the "Direction (°)" column reports the center of the Gaussian, the "Dispersion (°)" column reports the standard deviation of the Gaussian, the "Amount" column is the sum of the histogram from center-std to center+std, divided by the total sum of the histogram and the "Goodness" column reports the goodness of the fit, where 1 is good, 0 is bad.

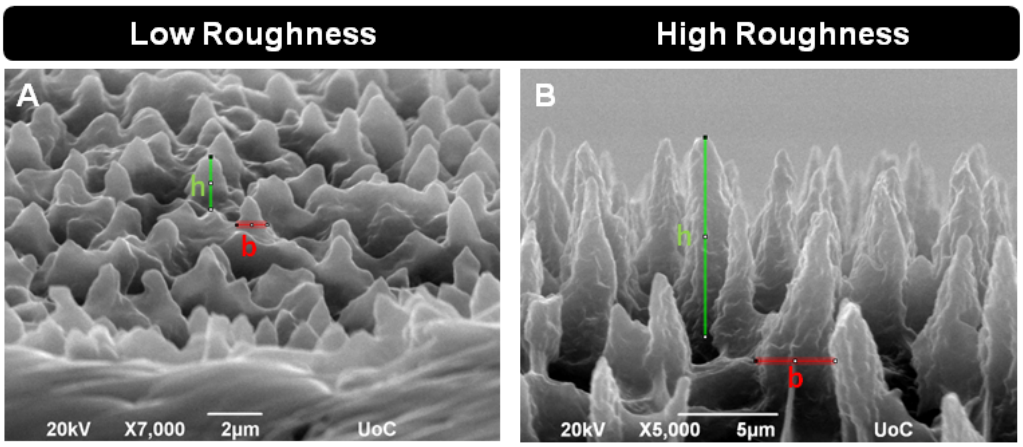

Figure 17: Cross section SEM images of low roughness (A) and high roughness (B) PCL replicas. A surface plot of each image was produced by Fiji ImageJ, and the height and spike's base were measured. From each image, at least 10 measurements were performed.

Table 2: Geometrical parameters of the spikes on low roughness and high roughness PCL replicas

PCL groups	Density [10^4/mm^2]	Height(h) [μm]	Width(b) [μm]	Aspect ratio
Low roughness	15.23±1.4	2.79±0.1	1.51±0.12	1.85
High roughness	7.21±0.4	8.53±1.3	3.23±0.05	2.7

In a previous study, poly(lactide-co-glycolide) (PLGA) was used instead of PCL to fabricate patterned surfaces via the soft lithography method, using exactly the same PDMS molds that were used at this thesis.[54] PLGA is a biocompatible and biodegradable synthetic polymer that is used to create patterned substrates for various applications in tissue engineering and regenerative medicine. From the results of that study, it turned out that the spikes of low roughness topographies had a height of 3.06±0.40μm and a width of 2.93±0.30 μm whereas, the spikes of high roughness topographies had a height of 10.55±1.10μm and a width of 4.68±0.41 μm. These differences in the height and width of the spikes on the two materials are not significant. However, comparing the spikes' density a significant difference arises. Specifically, density on low roughness PLGA was 7.18±1.30 and that on high roughness PLGA was 4.69±0.19. There results prove that PCL have a better replication ability than PLGA and, so the initial topography of Si masters has been transferred more accurately to PCL substrates.

Furthermore, polycaprolactone's excellent replication ability is confirmed by comparing PCL replicas geometrical characteristics with that of the initial Si masters (Tab.3). We notice that there are some small variations in the height and the width of the spikes but they are in the range of standard deviation errors.

Table 3: Geometrical characteristics of the spikes on the master Si master substrates as they were calculated from SEM images with the aid of Fiji-ImageJ.

Si masters	Height(h) [μm]	Width(b) [μm]
Low roughness	3.24±0.44	1.87±0.60
High roughness	8.63±1.17	4.78±1.05

3.1.3 Measurements of wettability of PCL replicas

In order to investigate how roughness and topography affect surfaces' wettability, the water contact angle of PCL substrates was measured (Fig18-19). At least 15 different samples of each PCL group were measured to obtain the average value and the results are summarized at Tab.3.

Table 4: Contact angle measurements of PCL patterned substrates

PCL substrate	Contact angle (°)
Flat	80±5
Low roughness	126±7
High roughness	superhydrophobic

According to literature, the water contact angle of a non-treated PCL surface is in the range of 74°-84° [77,78], and this is in complete agreement with the results of our measurements for flat PCL, which was 80°±5°. The contact angle of low roughness PCL was 126°±7°, whereas it wasn't possible to measure the contact angle of high roughness PCL and that's an evidence of its superhydrophobic character. Specifically, the droplet of water couldn't deposit on the surface effortlessly (Fig.19). A decrease in the hydrophilicity was observed from flat to high roughness PCL substrates, which is attributed to the increased roughness of the surfaces.

As it is aforementioned, surface free energy is directly related to surface wettability. In this work, surface free energy didn't directly measure. Water contact angle measurement alone indicates the wetting of the solid, but the surface free energy is the quantitative measure of the intermolecular forces at the surface. If we think about it in depth, the wetting ability of a solid is due to the interaction of the drop (usually water) with the chemical groups on the solid

surface. In case of PCL, weak Van der Waals forces and hydrogen bond are developed with the water drop and this justifies its hydrophobic nature. So, the lower a surface's free energy, the more hydrophobic it is.

The wetting properties of surfaces that are used in cell cultures, play an important role in cell adhesion. Hydrophilic surfaces can be coated with the proteins present in the medium and, thus allows cell attachment. However, latest studies have proved that surface topography promote cell adhesion regardless of wettability. Pegueroles et al[79], observed that topography on titanium surfaces has a more significant role in cell adhesion compared with wettability and surface free energy. In our study, two factors change; wettability and topography. So, a need arose to clarify which factor determines cell adhesion and, consequently, proliferation on PCL surfaces.

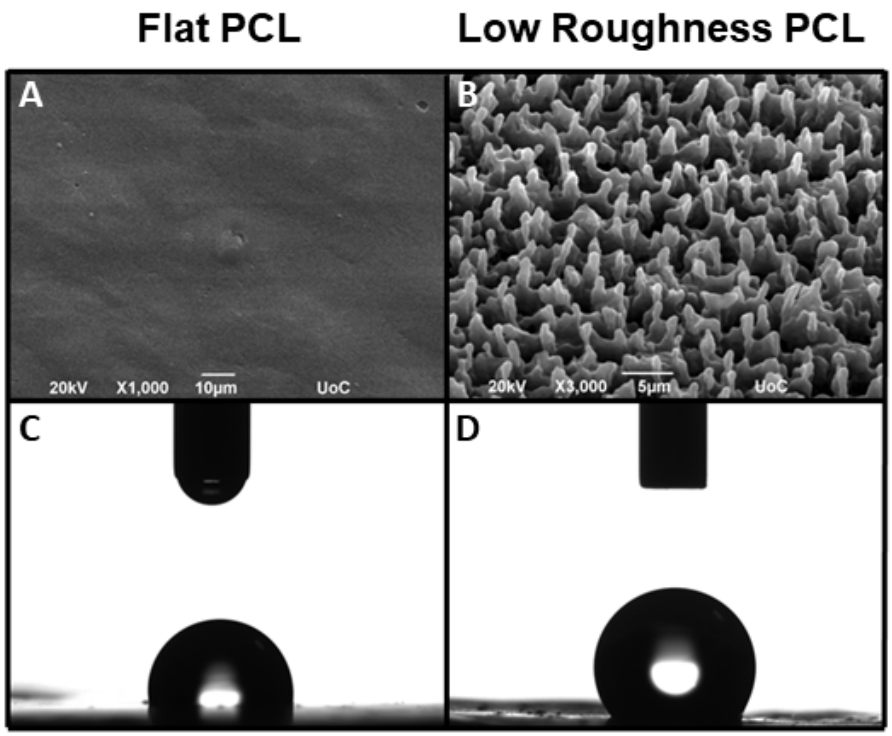

Figure 18: Tilted SEM images of flat (A) and low roughness (B) PCL replicas. Photographs of water droplets on (C) flat and (D) low roughness PCL replicas.

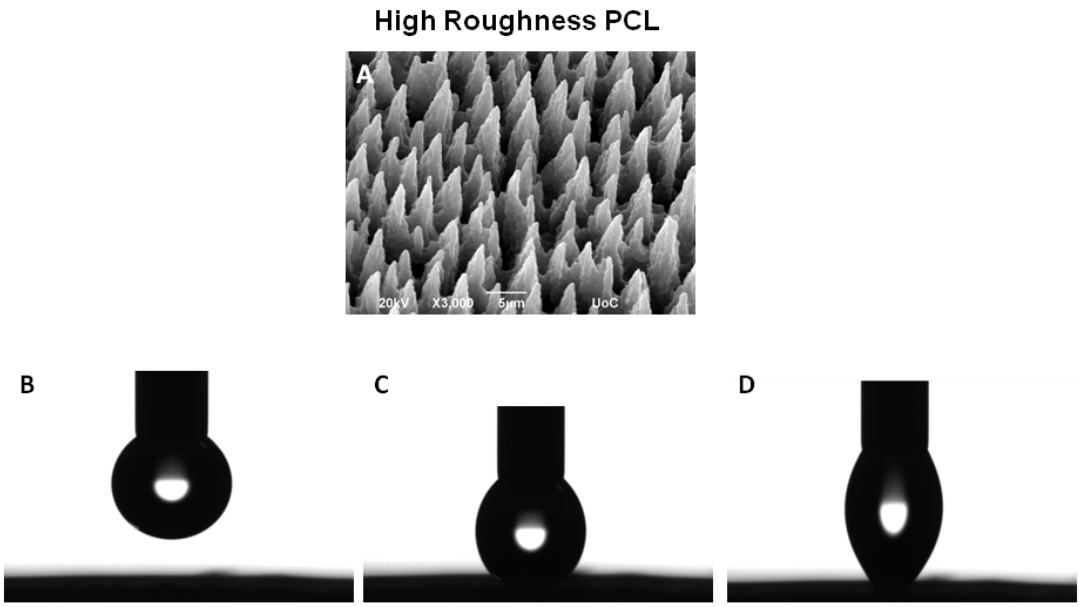

Figure 19: Tilted SEM image of high roughness PCL replica (A). The process of depositing the water droplet on high roughness PCL replica step by step (B-D)

3.2 Cell culture studies

3.2.1 Study of the identity and differentiation potency of MSCs with the expression of CD44 - a positive surface marker for MSCs

MSCs show differential morphology, growth rate, proliferation and differentiation potential depending on their source of origin and physicochemical cues such as cell culture media, fetal bovine serum, growth factors, as well as surface topography, interactions with surrounding cells and with components of the extracellular matrix used during the culture. So, there is a need to verify MSCs identity and multipotency both after isolation and after the cells have been passaged in culture.[67]

Mouse MSCs are generally characterized by the positive expression of CD44.[80] CD44 is a cell surface protein[81], form a large family of multifunctional, single-chain transmembrane glycoproteins belonging to the class of cell adhesion molecules (CAMs).[82] It interacts with a variety of ECM components, cytokines and growth factors and binding enables it to control cell signaling. It has been reported that CD44 surface markers of MSCs may bind to extra-cellular hyaluronic acid (HA) that exhibits various biological functions such like cell adhesion, matrix assembly, endocytosis and cell signaling.[83]

Thus, before using MSCs for all following studies, we had to check their identity and if they have the ability to differentiate. For this purpose, $5x10^4$/ml MSCs seeded on each PCL topographical category and on tissue culture plastic coverslip (TCP), which was used as a control sample. After 7 days of culture, immunofluorescence experiments were performed for the detection of the MSCs specific marker. As shown in Figure 20, MSCs on all the PCL surfaces

(flat and patterned) express the CD44 protein. This evidence affirms MSCs good function and, so, we continued with the study of MSCs response and behavior on PCL patterned and no-patterned surfaces.

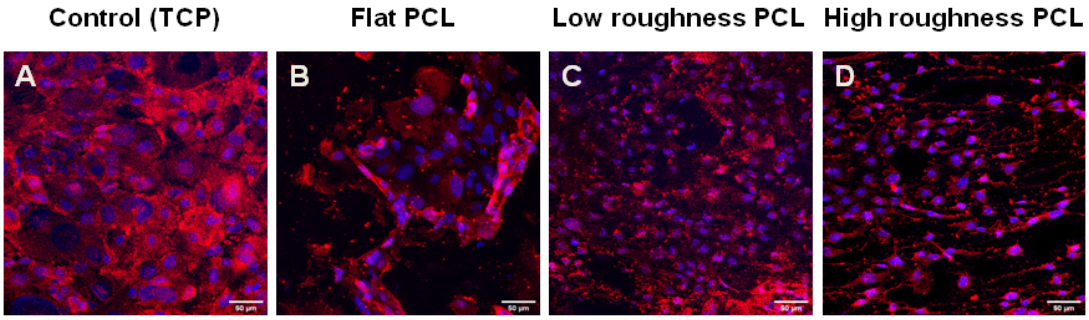

Figure 20: The CD44 (red) and nuclei (blue) staining of MSCs on A) Control (tissue culture plastic), B) Flat PCL, C) Low roughness PCL and D) High roughness PCL 7 days after seeding. Images were taken with confocal microscope.

3.2.2 Study of MSCs morphology by Scanning Electron Microscopy (SEM) and confocal microscopy

Several groundbreaking studies proved that cell morphology is sensitive to specific extracellular changes that cause cytoskeletal re-organization[84]. Historically, cell morphology has been used as an important indicator to characterize cell quality. D'Arcy Thompson was perhaps the first to postulate that cell shape has a physical and mechanical basis.[85] Maniotis et al.[86] proposed that cell shape information is transduced into gene expression through mechanical forces transmitted by the cytoskeleton. Nucleus shape and dimensions have also been shown to vary when cells are subjected to mechanical forces, while control of nuclear shape has been shown to induce osteocalcin expression in isolated pre-osteoblasts. [84,87]

Nowadays, technological development in the field of micro-nanopatterning gives the opportunity for controlling cell shape rather than merely interpreting it. In many studies, patterned substrates have been used to investigate the relationship between shape and differentiation of multipotent MSCs.[88,89,90] Chen et al. [91] recently demonstrated the important role that cell shape and size can play in directing the fates of MSCs. Although they descend from a common mesenchymal stem cell precursor, differentiated adipocytes are round and fat-laden, while osteoblasts vary from elongated to cuboidal, depending on their matrix deposition activity.[92] The shapes of these cells serve their specialized functions, while simultaneously driving their multicellular organization. A round, spherical shape allows for maximal lipid storage in adipose tissue, while cell spreading facilitates osteoblast matrix deposition during bone remodeling. These different cell morphologies are thought to arise from changes in the expression of integrins, cadherins, and cytoskeletal proteins during stem cell commitment, the process by which a cell chooses its fate and differentiation.

Osteogenic cells have a highly developed cytoskeleton and it is known that their differentiation is regulated in part through mechanical forces imposed by their surrounding environment.[93] Osteocytes are the most numerous of bone cells, derived from a select group of osteoblasts that have undergone a final differentiation and are left behind, encased within the mineralized bone matrix[94]. Osteoblasts initially become rounded during the differentiation process before they are embedded in the mineral matrix to become dendritic osteocytes.[95] Changes in cell morphology have recently been shown to affect both intracellular stress and osteoblast differentiation.

In this study, morphological differentiations of multipotent MSCs cultured on three types of patterned and non-patterned PCL scaffolds were observed by SEM and confocal microscopy. In addition, MSCs were seeded on tissue culture plastic coverslips (polystyrene), which is the material of cell culture dishes and considered as control. The conditions of culture were the same for all surfaces, the density of cells seeded was $5x10^4$ cells/ml and no growth factors were added (culture in standard medium, as described in chapter 2.2.1).

In the case of SEM, cells were prepared with the dehydrated procedure, as described above (chapter 2.2.2). The advantage of SEM in relation to confocal microscope is that besides the morphology of cell body and the formation of filaments the underlying topography can also be observed. As shown in Fig.21, MSCs present a range of different morphologies at each topographical type and TCP, but if they are observed very carefully, there are only five cell shapes which are repeated (Fig.22).

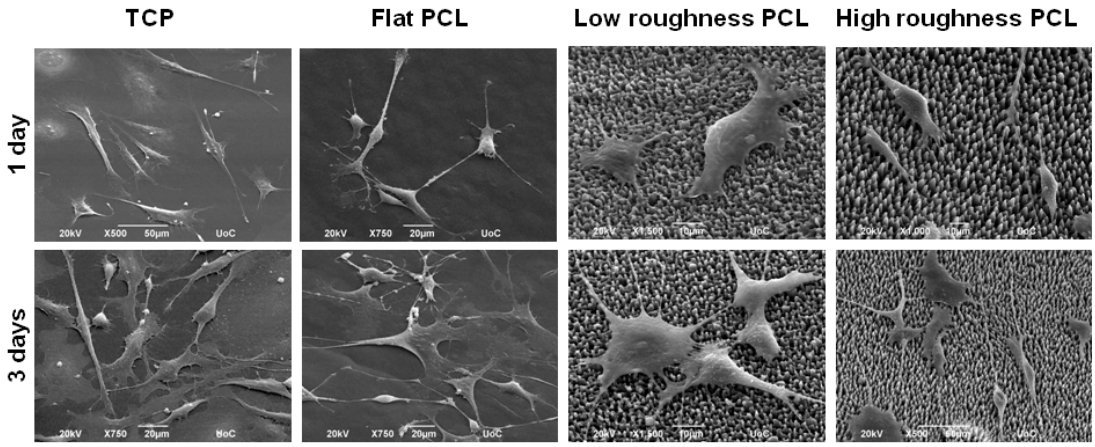

Figure 21: SEM images of MSCs morphologies on tissue culture plastic (TCP) coverslips, flat, low roughness and high roughness PCL scaffolds 1 and 3 days after seeding ($5x10^4$ cells/ml).

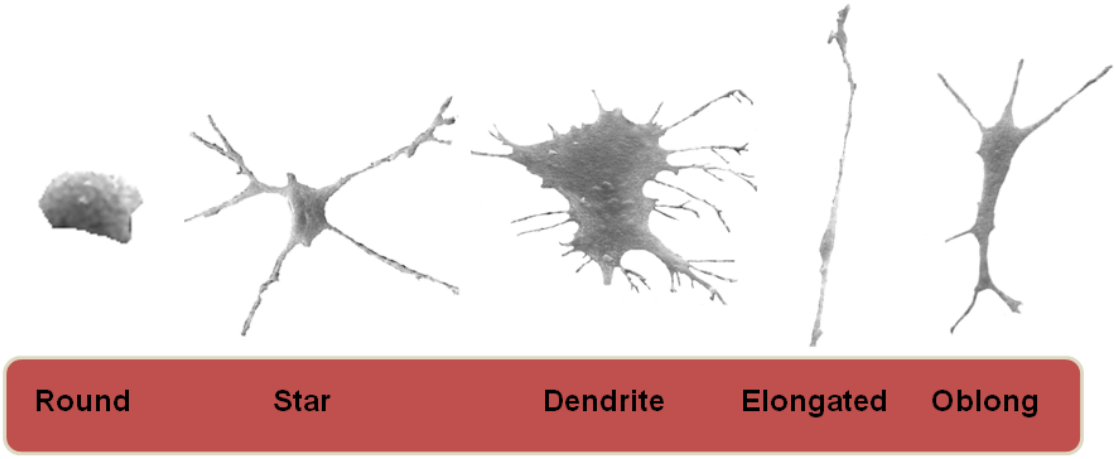

Figure 22: Morphological types of MSCs on PCL scaffolds. Cell outlines emerged from SEM images.

However, due to the fact that cell nucleus and cytoskeleton are not detected in SEM images, confocal microscopy was used for the study of the MSCs morphology. Thus, the nuclear staining carried out by DAPI and the cytoskeletal staining held with phalloidin (chapter 2.2.5) (Fig.23).

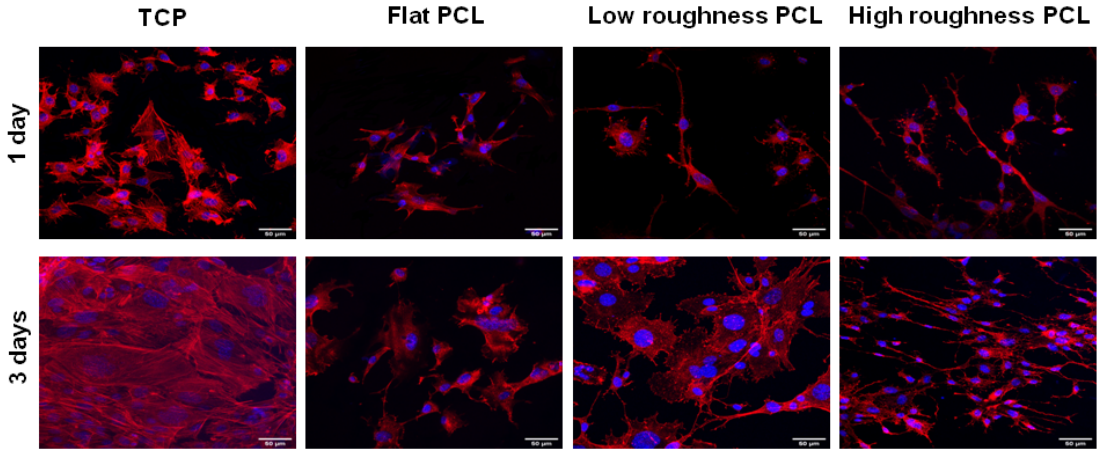

Figure 23: Confocal microscope images of MSCs morphologies on tissue culture plastic (TCP) coverslips, flat, low roughness and high roughness PCL scaffolds 1 and 3 days after seeding ($5x10^4$ cells/ml).

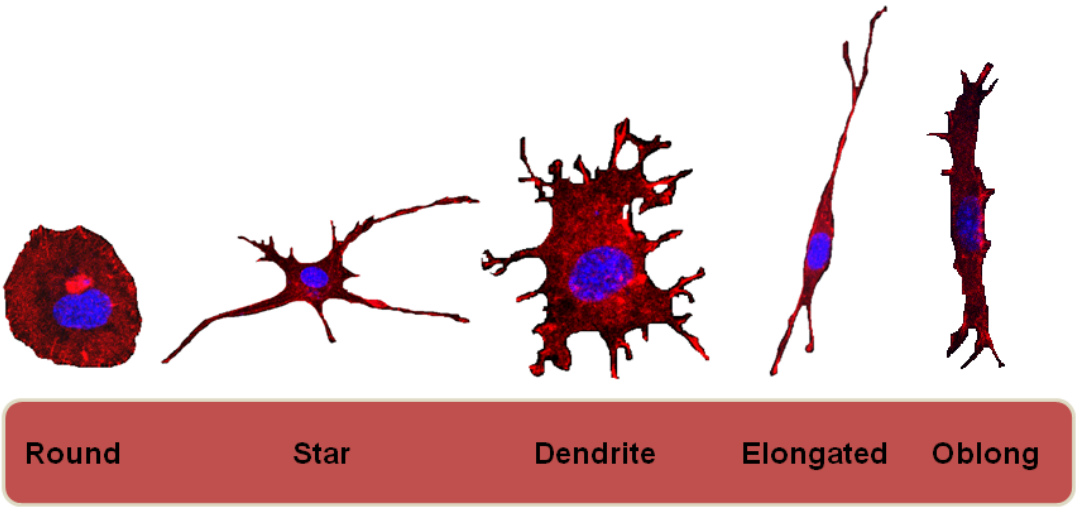

Figure 24: Morphological types of MSCs on PCL scaffolds. Cell outlines emerged from confocal microscope images. The cytoskeleton was stained with phalloidin (red) and the nucleus with DAPI (blue).

As it turned out both from SEM and confocal microscopy results, there are five predominant morphological types of MSCs; the round, the star-like, the dendrite, the elongated and the oblong. The MSCs were categorized by taking into account three criteria; nucleus diameter, cell body axis and number of filopodia (Tab.4). Specifically, it is observed that round and star types have a similar cell body size, but the star has, also four-five filaments. The dendrite has bigger cell body and nucleus diameter than the round and the star and has many filaments, perimeter throughout the body. Comparing the elongated and the oblong types the main difference is that the oblong has bigger cell body axis and no filaments, in contrast to the elongated that has smaller cell body and very thin filaments (Fig.24).

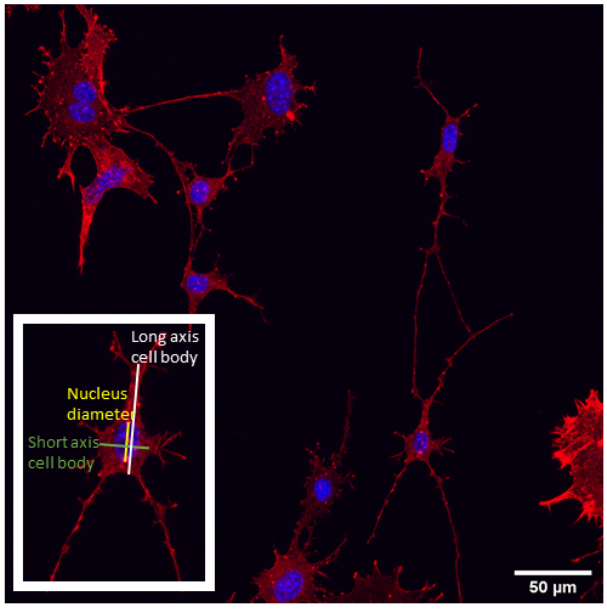

Figure 25: An example of how we measured nucleus diameter, long and short axis cell body (This is a random example of a high roughness PCL sample)

Table 5: Cell's measurements of the five morphological types of MSCs on PCL scaffolds. Cell aspect ratio defined as the ratio of the length of the long axis cell body to the length of the short axis cell body. All measurements were performed with Fiji ImageJ from a total of at least 30 cells of each morphological group.

	Round	Star	Dendrite	Elongated	Oblong
Nucleus diameter [μm]	12±2	16±4	20±6	12±2	20±4
Long axis cell body [μm]	39±12	54±15	73±22	38±14	99±27
Short axis cell body [μm]	18±3	22±5	37±11	13±3	23±7
Cell aspect ratio	2.17	2.45	1.97	2.92	4.30

Later on, cells of each category on flat, low and high roughness PCL scaffolds were counted so as to find which type prevails on the three different topographical surfaces. Cell counting was held 1 and 3 days after cell culture and the results are summarized in Fig.26 and Fig.27. In detail, on flat PCL surfaces the round, the star and the oblong have a similar rate while the elongated presents the smallest and the dendrite presents the largest rate. On low roughness PCL surfaces things are clearer because there is a wide range between the rate of dendrite and the rates of the rest four types. On high roughness PCL surfaces the elongated has the biggest rate, but the round and the dendrite have a remarkable rate, too. Summarizing the results for the first day after culturing, only on low roughness PCL surfaces there is clear evidence, while on flat and high roughness all morphological types have a satisfying occurrence rate. As shown in Fig.27, the dendrite is the predominant morphological type for all the PCL surfaces three days after cell culturing. However, the rate of the elongated cells is remarkable on high roughness PCL.

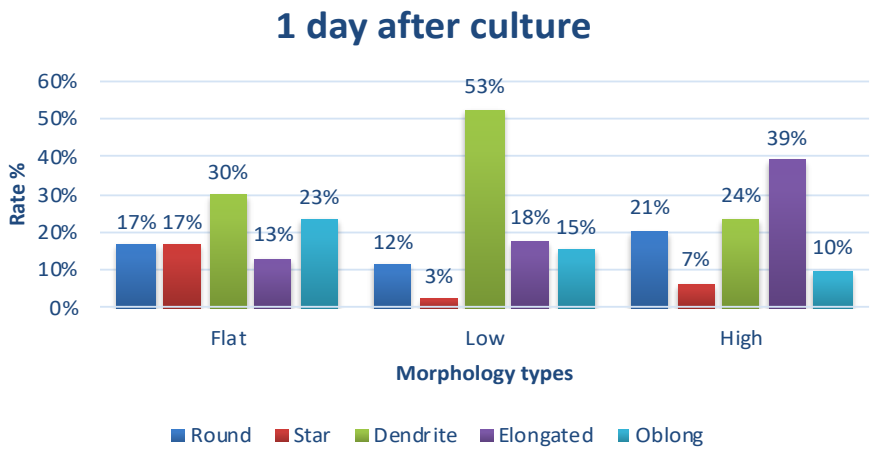

Figure 26: Statistical results from the occurrence rate of each morphological cell type after one day of cell culture on flat, low and high roughness PCL scaffolds. The results were extracted from at least 20 samples from each category of PCL scaffolds.

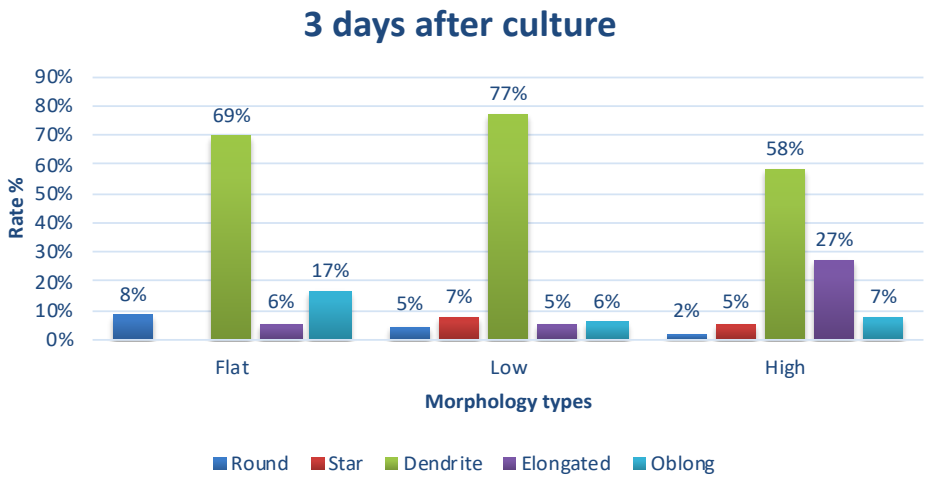

Figure 27: Statistical results from the occurrence rate of each morphological cell type after three days of cell culture on flat, low and high roughness PCL scaffolds. The results were extracted from at least 20 samples from each category of PCL scaffolds.

According to Tab.4 and cell aspect ratio results, all MSCs morphological types are anisotropic (cell aspect ratio >1). Cell shape anisotropy or polarity in cells is critical and has been suggested to play a pivotal role in determination of cell differentiation. Previous studies indicate that cell elongation (increasing cell aspect ratio) could be a factor that facilitates differentiation of MSCs, even without the external chemical induction factors.

Wagner and co-workers[34] and Ding and co-workers [96] independently showed that there is a dependency between the cell aspect ratio and osteogenic differentiation. Wagner et al., found that stem cells grown on microgrooves with high cell aspect ratio (~10) showed enhanced osteogenic differentiation, whereas Ding et al. showed that osteogenic differentiation was optimal for cells with cell aspect ratio of about 2. Mrksich and co-workers[97] summarized that "the yield of osteogenesis increased with aspect ratio", but this comes into complete controversy with Ding and co-workers findings. Yang and co-workers[98] suggest that there is a limit to what extent elongation is beneficial. From the above it turns out that changes in cell morphology and so, changes in cell aspect ratio and isotropy determine intracellular mechanics, dynamics and forces and thus modulate cell differentiation.[99] However, we can't predict cell's fate only by its shape because cell differentiation is determined by many combinational factors, like mechanical stimuli, focal adhesion maturation, surface stiffness, etc.

According to literature, osteocytes have a characteristic stellate shape (Fig.28) that is similar with the dendrite shape. Taking into account all the aforementioned, we can't declare that MSCs will differentiate to osteocytes only with this evidence, but we state that shape determines specialized cell functions and cell differentiation.

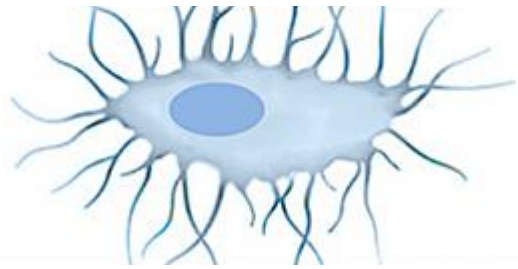

Figure 28: Typical osteocyte morphology

3.2.3 Study of Mesenchymal Stem Cells (MSCs) adhesion on polycaprolactone (PCL) scaffolds

It is widely accepted that cells adhere to substrates through focal adhesions (FAs) complexes, which contain hundreds of different proteins and their composition changes in response to physical stimuli, making them important

sites of mechanotransduction. Thus, FAs are multifaceted organelles that mediate an array of functions involving biochemical and physical interactions between the cell and its environment. [100]

Vinculin is a mechanosensitive cytoskeletal protein which is recruited to FAs and plays an important role in multiple FA functions, including cell adhesion strengthening and stabilizing, ECM mechanosensing and regulation of actin cytoskeletal dynamics.[101] The spatiotemporal regulation of different vinculin interactions seems to regulate cellular function.[102] Structurally, vinculin comprises three major domains: a N-terminal head, a flexible proline-rich hinge (neck) region and a C-terminal tail domain. Vinculin activation results from conformational rearrangements of these domains. Vinculin, via the interaction of its tail with actin, is the major link of the FA core to the actin cytoskeleton.[103]

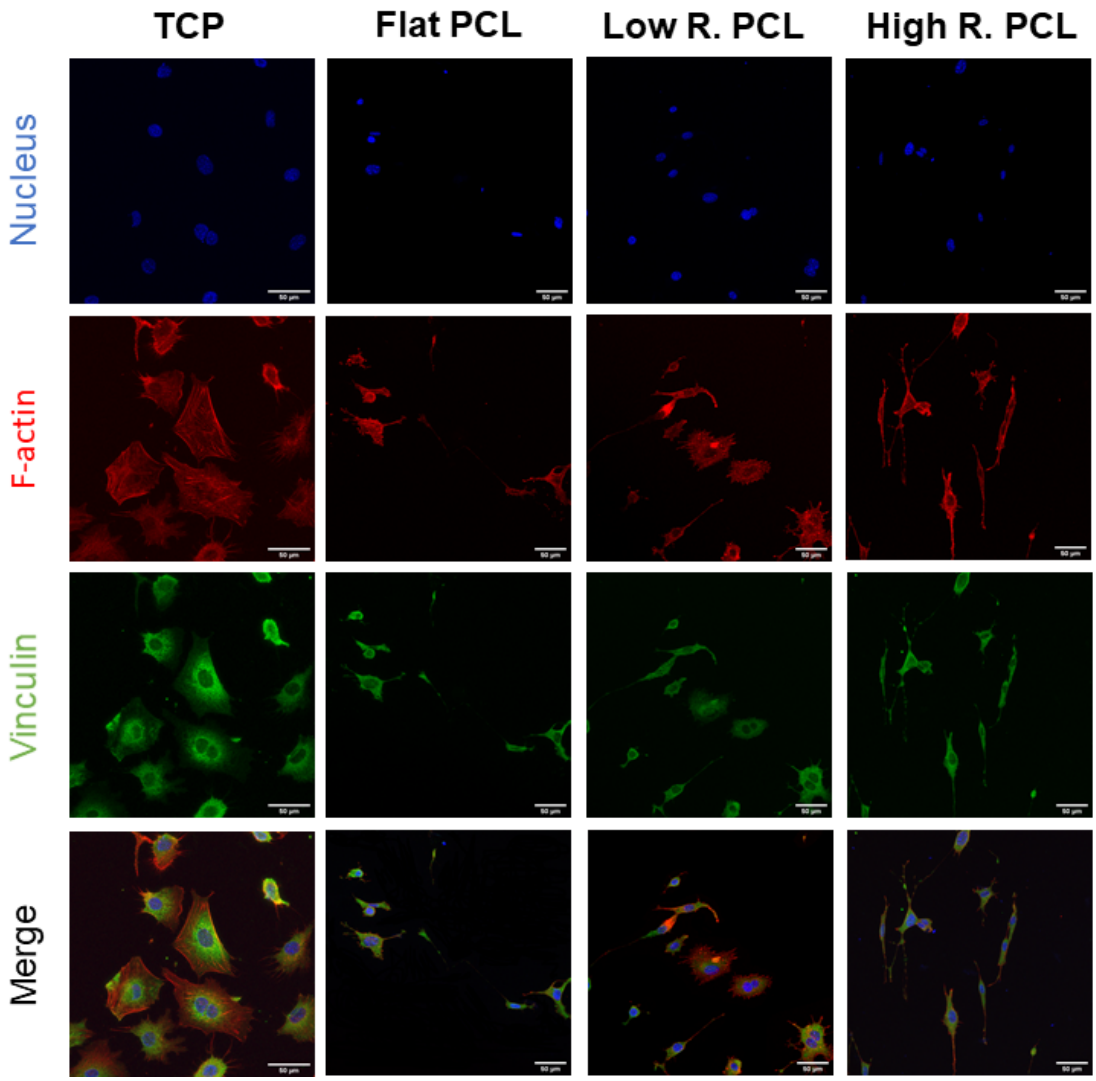

Figure 29: Confocal microscope images of MSCs on tissue culture plastic (TCP) coverslips, flat, low roughness and high roughness PCL scaffolds 1 day after seeding ($3x10^4$ cells/ml). (Blue: staining of cell nucleus with DAPI, Red: staining of cells F-actin with TRITC, Green: staining of vinculin-adhesion points)

In order to evaluate the ability of MSCs to adhere on micro-structured surfaces and to better understand how the topographic cues modulated cellular morphology, we stained cells for the actin cytoskeleton and the focal adhesion protein vinculin. Thus, cells seeded with the density of $3x10^4$ cells/ml on flat, low roughness and high roughness PCL, as well as on tissue culture plastic (TCP) coverslips for 1 day, as described above (chapter 2.2.1). As shown in Fig.29, vinculin was expressed throughout MSCs body and filaments on TCP and all PCL topographies. It is, also, clear that different cell morphologies appear on each PCL group and on TCP, too. As it is aforementioned, cells cytoskeleton is re-organized by receiving mechanical forces from the ECM via signal transmitting structures, like vinculin. Thus, it turns out that cell shape and morphology on the patterned and non-patterned substrates are directly connected to selective vinculin expression.

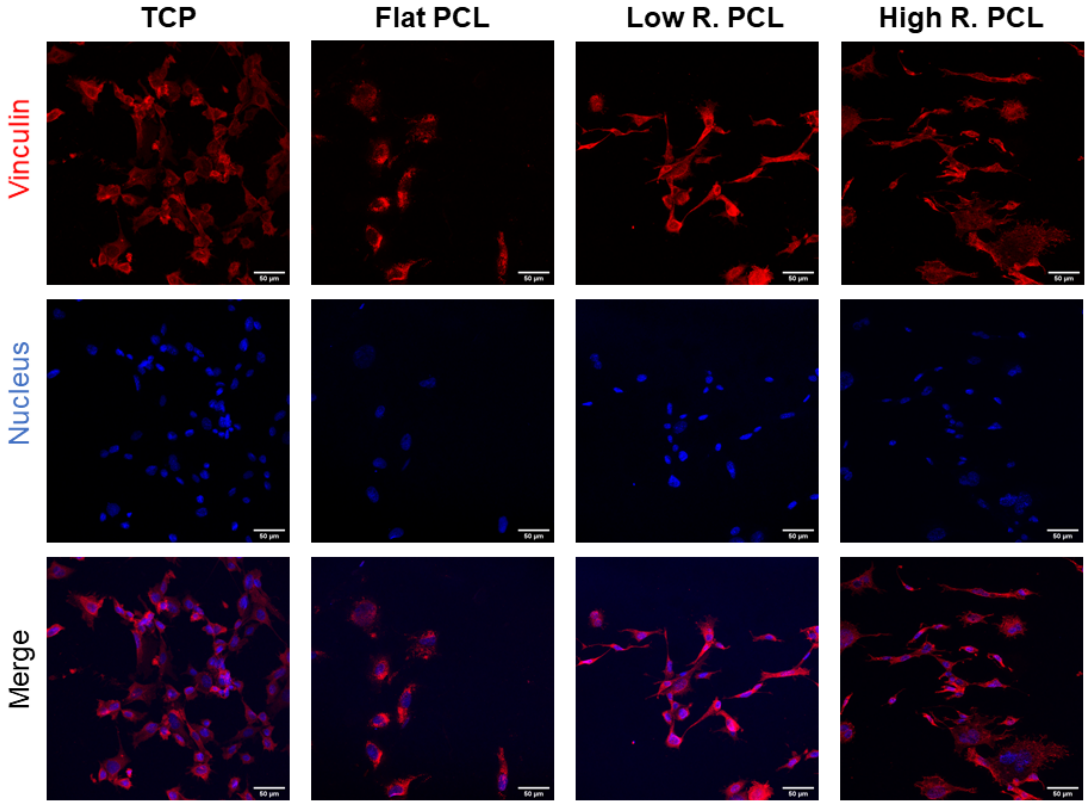

Figure 30: Confocal microscope images of MSCs on tissue culture plastic (TCP) coverslips, flat, low roughness and high roughness PCL scaffolds 1 day after seeding ($5x10^4$ cells/ml). (Blue: staining of cell nucleus with DAPI, Red: staining of vinculin-adhesion points)

Furthermore, we studied in detail if there is a difference in fluorescence intensity of vinculin between PCL topographical groups and if vinculin expression is more intense on some points of cells than on others. At this part of the study, cells seeded with the density of $5x10^4$ cells/ml on all PCL groups and TCP for 1 and 3 days and vinculin expression was stained. The results of the first day after culture are summarized in Fig.30 and it is observed that there is higher fluorescence intensity of vinculin perimeter of the MSCs nuclei on TCP and flat

PCL, whereas on low and high roughness PCL it is observed an equal distribution of vinculin fluorescence intensity both in MSCs body and filaments. Three days after culture (Fig.31) this difference between the PCL groups is clearer. It is hypothesized that this selective vinculin expression is directly related to topographical cues. The finding that vinculin is differentially regulated on micro-topographies strongly suggests that cellular functions, especially mechanotransduction, may be controlled by the modulation of topographical cues at the microscale.

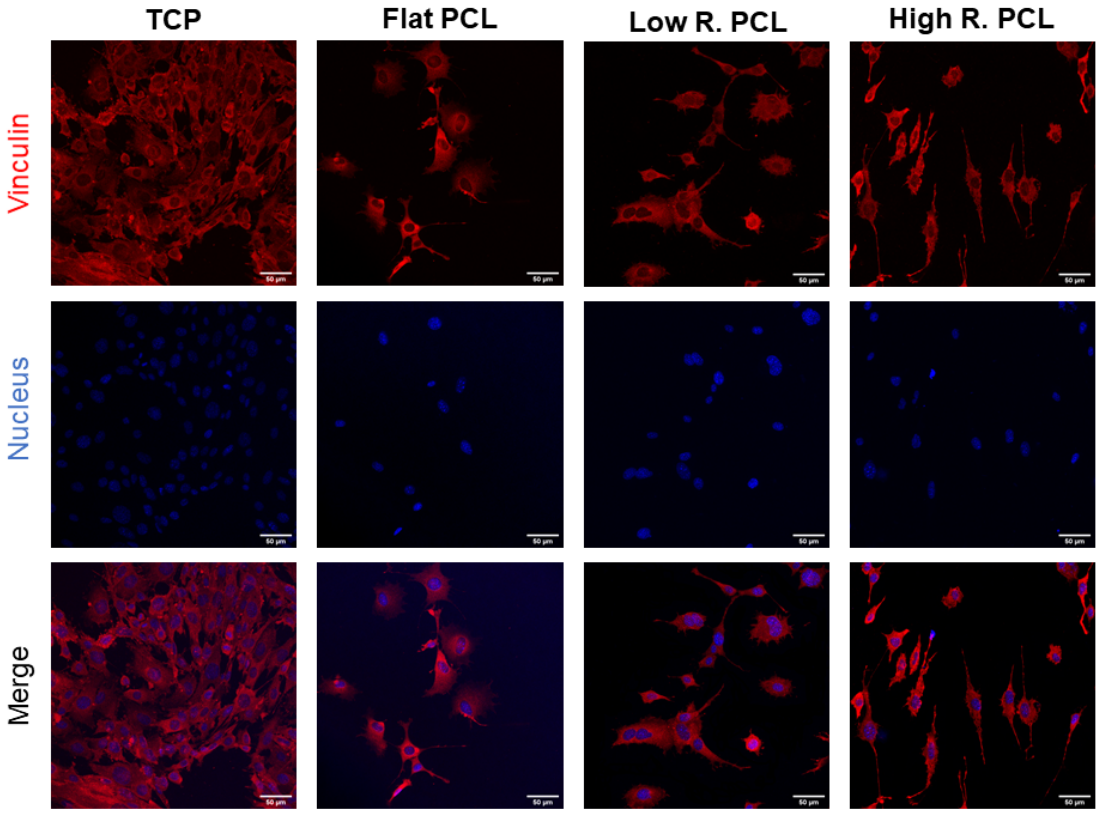

Figure 31: Confocal microscope images of MSCs on tissue culture plastic (TCP) coverslips, flat, low roughness and high roughness PCL scaffolds 3 days after seeding ($5x10^4$ cells/ml). (Blue: staining of cell nucleus with DAPI, Red: staining of vinculin-adhesion points)

Later on, we calculated the vinculin fluorescence intensity for the three PCL groups with Fiji ImageJ (plugin "Measure") (Fig.32). After measuring the integrated density, we used the following formula to calculate the corrected total cell fluorescence (CTCF) and the results are shown in Fig.33. (This method is based on an original protocol from QBI, The University of Queensland, Australia).

- CTCF = (Integrated Density/Area of selected cell) - Mean fluorescence of background readings

As shown in Fig.3, at day 1, vinculin fluorescence intensity is highest on low roughness PCL, while flat and high roughness PCL have a similar vinculin intensity. So, this is an evidence that MSCs adhere strongly on patterned low roughness PCL surfaces that on flat and high roughness. Three days after culture, it is observed a decrease in intensity, mainly for low roughness PCL, whereas in flat and high roughness PCL the intensity is almost the same. This is a result that we expected because, according to literature, vinculin acts at the early stage of focal adhesion formation and then its expression decreases.

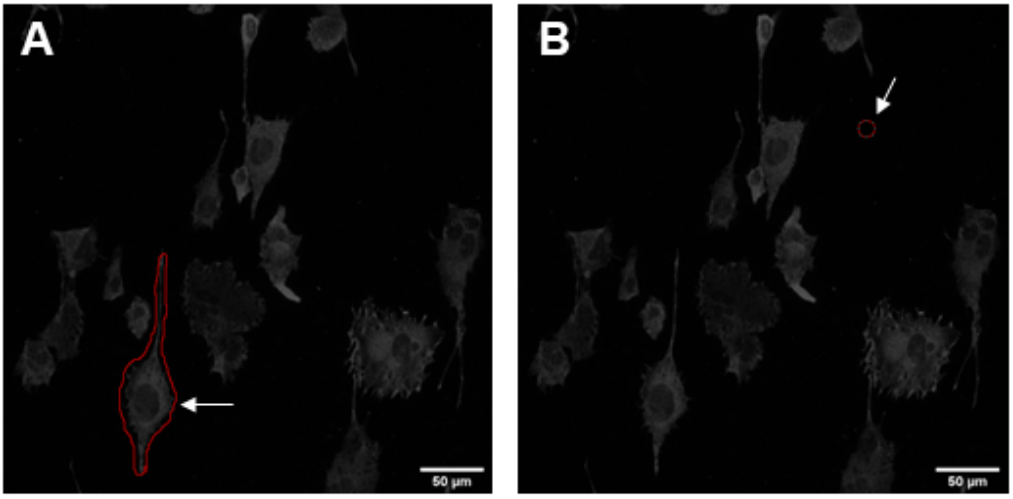

Figure 32: An example of how vinculin fluorescence intensity was calculated on Fiji ImageJ. At least 15 cells were measured for each PCL group and for each time point and from three independent experiments. A) Selection of the cell of interest using the drawing tools. B) Selection of a region which will be considered as background. (This is a random example of a high roughness PCL sample 3 days after culture).

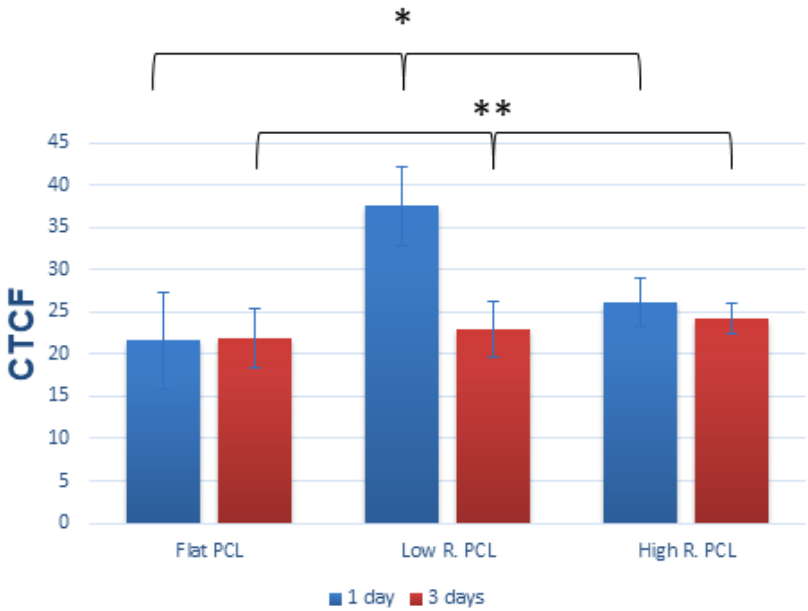

Figure 33: Vinculin fluorescence intensity at 1 and 3 days after MSCs culture on flat, low and high roughness PCL substrates. The data were subjected to ANOVA with post hoc Tukey HSD test for multiple comparisons between the groups. (*$p<0.0004$, **$p<0.01$)

3.2.4 Effect of flat and patterned PCL substrates on MSCs proliferation

To investigate the effect of surface topography on cell proliferation, MSCs seeded at the same cell density (5 x 10^4 cells/ml) on flat, low and high roughness PCL scaffolds for 1, 3 and 7 days as described above (chapter 2.2.1). Samples were observed under the confocal microscope and the results analyzed with Fiji ImageJ. Specifically, cells' nuclei were stained with DAPI and the plugin "Analyze particles" on Fiji ImageJ was used to count cells on each of the three topographical PCL categories (Fig.34). A total of at least 15 samples were counted for each topographical category and for each time point and the results are summarized at Fig.35.

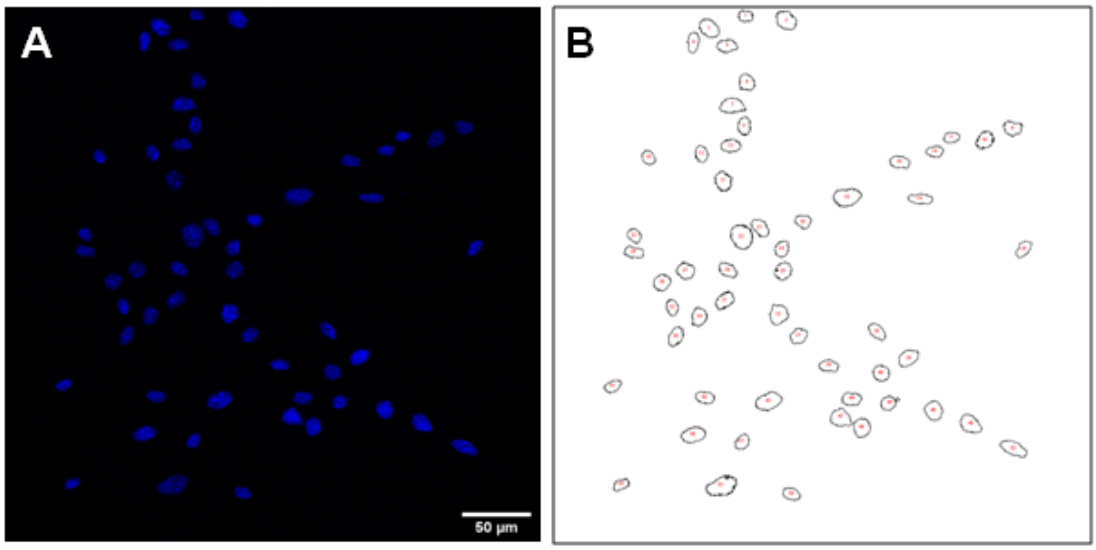

Figure 34: Cell counting example. A) Cell nuclei were stained with DAPI and observed under confocal microscope (This sample is a random high roughness PCL scaffold three days after cell seeding). B) The result of "Analyze particles" on Fiji ImageJ.

As shown in Fig.35, the highest density of cells 1 day after culture was found on high roughness surfaces and the smallest on flat PCL. In particular, the number of cells on low roughness PCL is almost double than that on flat and the number of cells on high roughness PCL is almost double than that on low roughness PCL. Three days after seeding, MSCs density on low and high roughness PCL is almost the same and double compared to that on flat PCL. Seven days after seeding, the biggest density of MSCs was found on low roughness PCL, while the smallest density appeared on flat PCL. Comparing the three topographical types, it turned out that MSCs prefer the spikes-patterned PCL to adhere and proliferate on, in contrast to the no-patterned flat PCL. Furthermore, the cell volume coverage on each topography is affected by the time points, due to cell spreading/migration and proliferation.

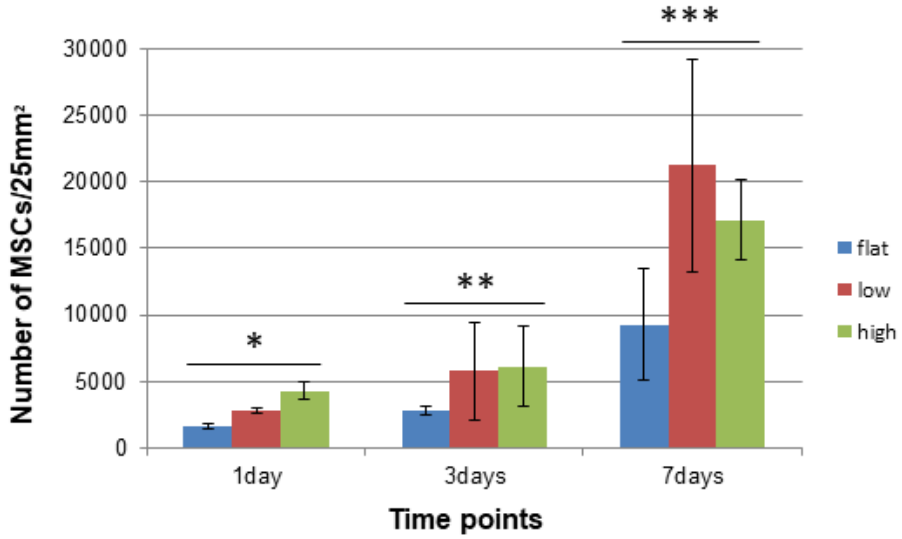

Figure 35: MSCs proliferation on flat, low and high roughness PCL scaffolds 1, 3 and 7 days after cell seeding. As mentioned, PCL-patterned surfaces have a size area of 5x5mm (=25mm^2) and so cell density is expressed as number of MSCs/25mm^2. The data were subjected to ANOVA with post hoc Tukey HSD test for multiple comparisons between the groups. (*$p<0.01$, **$p<0.05$, ***$p<0.08$)

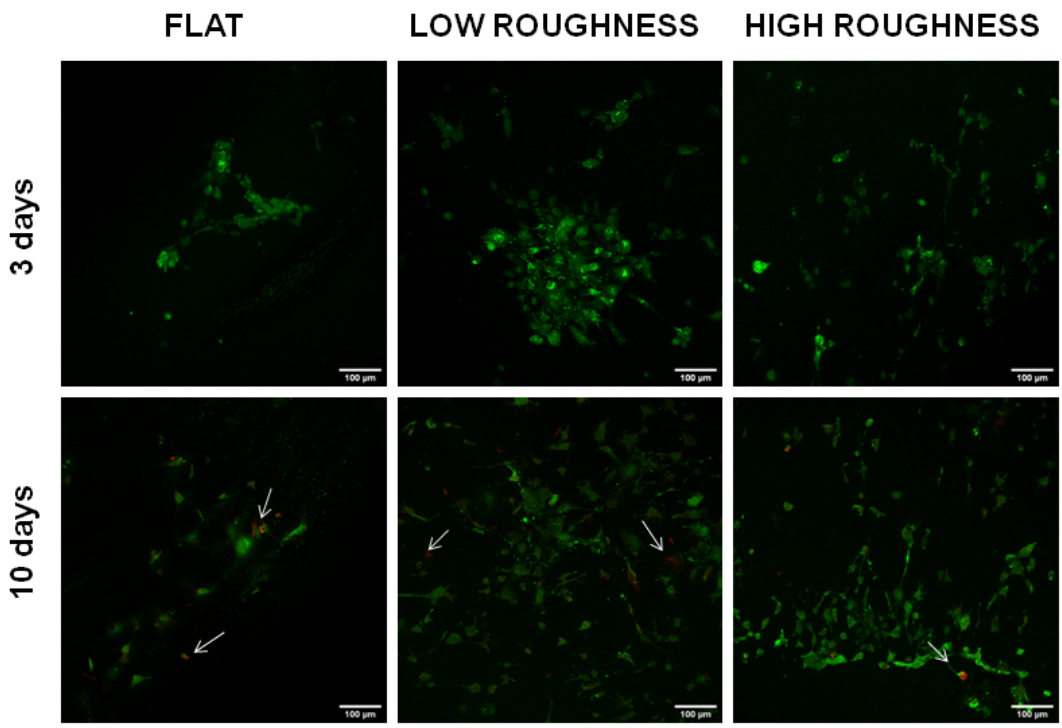

Figure 36: Confocal images of Live/Dead assay 3 and 10 days after cells seeding on flat, low and high roughness PCL substrates. Green: calcein, Red: ethidium homodimer-1 (EthD-1). The white arrows indicate dead cells.

In order to examine what happens with cell proliferation and whether the low density of cells on flat PCL is due to possible cell death, a Live/Dead™ Viability/Cytotoxicity assay was performed. MSCs were seeded on flat, low and high roughness PCL at a density of 3x10^4 cells/ml and cultured for 3 and 10 days. As shown in Fig.36, there are some dead cells in 10 days of cell culture

not only on flat PCL but on all PCL topographical categories; however, the number of dead cells is completely normal and comes to an agreement to cell cycle. So, this additional study complements the results of proliferation and reinforces the conclusion that MSCs proliferate to a greater extent on low and high roughness PCL than on no-patterned PCL.

3.2.5 Study of Mesenchymal stem cells (MSCs) mechanoresponse to substrate roughness and stiffness

Stiffness (or rigidity) is the ability of substrate to resist mechanical force applied to it.[104] Our tissues, which are composed of a variety of different ECM molecules, feature a wide range of elastic moduli, and each tissue has specific stiffness for fulfilling physiological needs. For example, bone is much stiffer than other tissues, because its primary function is to provide structure and protect our internal organs.[105]

Roughness and stiffness of the extracellular matrix (ECM) changes cell adhesion, proliferation and differentiation. An important discovery in 2011 by Dupont et al.[106] showed that cells read ECM elasticity, cell shape and cytoskeletal forces as levels of Yes-associated protein (YAP) activity.[107,108] YAP is a transcriptional activator and acts as key regulator for mechanotransduction, through its localization which is very indicative for how the cell perceives mechanical properties and topography.[98,109] It has been reported that YAP is imported into the nuclei when cells are cultured on rigid substrates,[110] whereas it is exported to the cytoplasm, phosphorylated, and degraded via the proteasome system on elastic substrates.[111]

Most of the studies to understand effect of stiffness on stem cells have been performed using MSCs, as they are able to differentiate into cells (osteocytes, chondrocytes, myocytes, neurons) that have dramatically different ECM stiffness. Previous studies have shown that stem cells cultured on stiff substrate (<30–70 kPa) organize F-actin bundles, generate cytoskeletal tension, which leads to translocation of YAP into nucleus for downstream gene activation for osteogenesis.[108] On the other hand, when MSCs cultured on soft substrates (0.3–3 kPa), YAP was found in the cytoskeleton due to the lack of cellular tension and adipogenesis was favored.[112]

In the present study, the transcriptional activity was analyzed by investigating the activation of YAP. Thus, MSCs seeded on TCP, flat, low and high roughness PCL with the density of $5x10^4$ cells/ml and 1 day after culturing, YAP expression was stained and the results are presented in Fig.37. Cells stained for YAP showed higher nuclear localization on high roughness PCL and TCP compared to flat and low roughness PCL. It is observed that the level of YAP nuclear accumulation increased with the stiffness and roughness increasing.

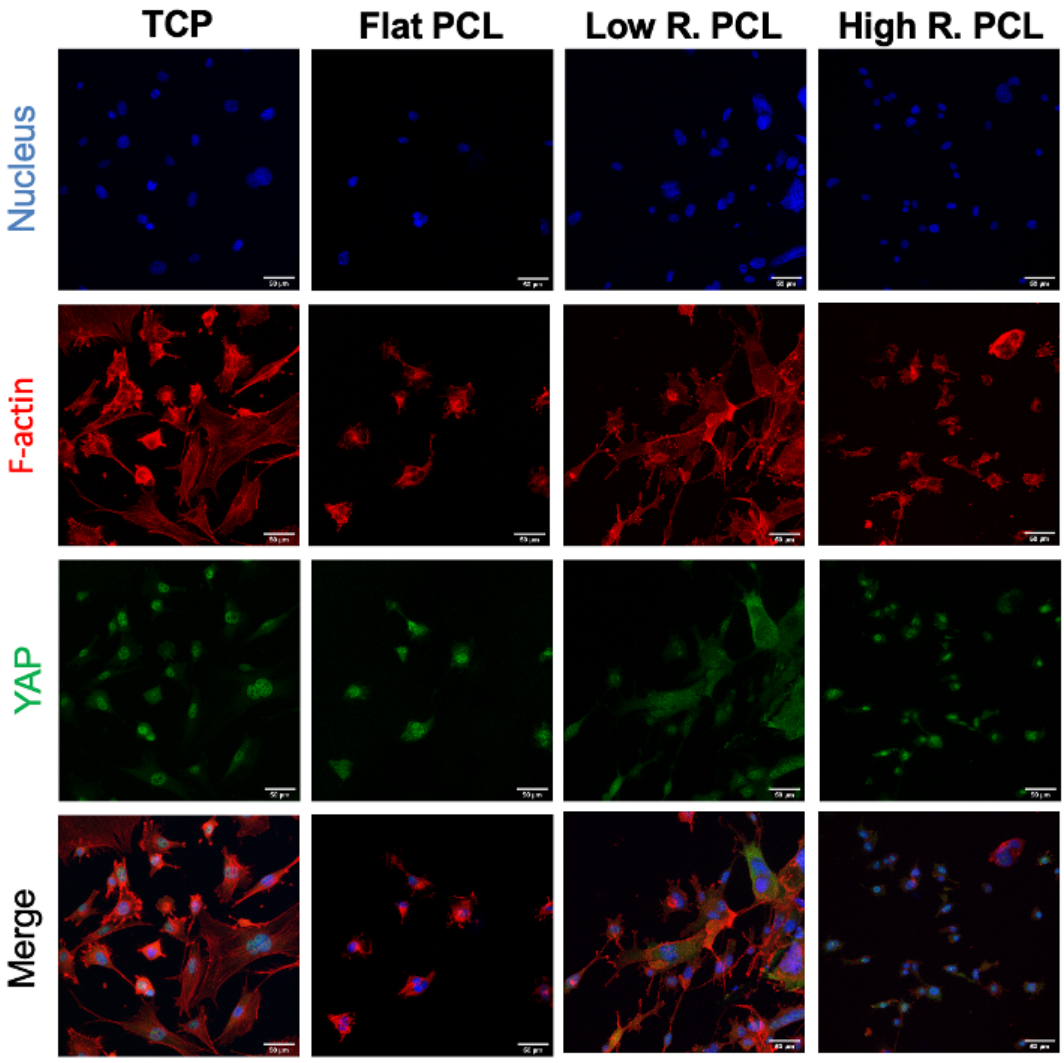

Figure 37: Confocal microscope images of MSCs on TCP coverslips, flat, low roughness and high roughness PCL scaffolds 1 day after seeding ($5x10^4$ cells/ml). (Blue: staining of cell nucleus with DAPI, Red: staining of cells F-actin with phalloidin, Green: YAP expression staining).

Table 6: Literature information for PCL[113,114] and polystyrene (TCP) mechanical properties. TCP mechanical information is given from the constructor.

	Tensile strength (MPa)	Elongation at break (%)	Young's modulus (MPa)
PCL	16.9±1.2	393±25.0	429.1±24.8
Polystyrene (TCP)	46	3.4	3250

Previous studies suggest that exogenous mechanical inputs from the microenvironment are transduced through the actin cytoskeleton to the nuclear envelope, and that stress in the nuclear envelope physically stretches nuclear pore complexes to bias nuclear import of key transcriptional co-activators like YAP. These data support that YAP nuclear translocation does not depend on

the contractile state of the cell per se, but rather depends on the transfer of contractile strain energy to the nucleus and generation of stress in the nuclear envelope.

Cosgrove et al.,[115] studied 2D hydrogel platforms and they found that the degree of nuclear envelope (NE) wrinkling in mesenchymal cells can predict their focal adhesion maturation state and YAP nuclear localization. Nuclear envelope wrinkling was evident when MSCs were cultured on soft planar 2D substrates, whereas nuclear wrinkling decreased significantly as hydrogel stiffness increased. They, also, found that wrinkled nuclei had significantly lower YAP nuclear/cytoplasmic ratio, indicating that shuttling preferentially occurs when nuclear envelope wrinkling is low and the nuclei are taut.

Subsequently, the YAP nuclear/cytoplasmic ratio was determined by dividing the average YAP fluorescence intensity in the nuclei by the average YAP fluorescence intensity in the cytoplasm. Images from three individual experiments and at least five samples of TCP and each PCL group were used and the average value for each image was recorded.

As shown in Fig.38., the high roughness PCL presents the highest nuc/cyt YAP ratio, followed by TCP, whereas low roughness PCL has the smallest ratio with no significant difference from flat PCL. Taking into account the Young's modulus and mechanical properties of TCP and PCL (Tab.4), TCP is harder than PCL. These results indicate that increasing roughness affects stronger than stiffness YAP nuclear localization.

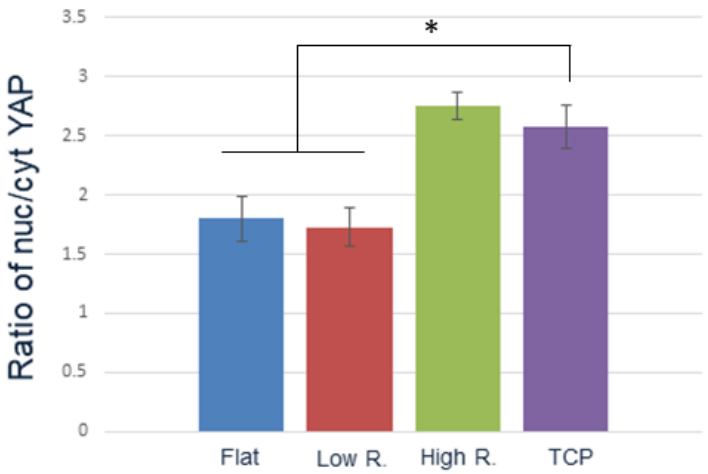

Figure 38: Quantification of the ratio of nuclear YAP to cytoplasmic YAP 1 day after MSCs seeding on TCP, flat, low and high roughness PCL. The data were subjected to ANOVA with post hoc Tukey HSD test for multiple comparisons between the groups (*$p<0.05$).

3.2.6 Alkaline phosphatase activity

MSCs morphological study (see chapter 3.2.2) and YAP activity (see chapter 3.2.5) results claim that MSCs that grow on patterned substrates prefer to differentiate into osteocytes. So, the need arose to investigate MSCs profile on PCL substrates. ALP activity assay is one of the most common studies to evaluate the extent of osteoblast differentiation and its increased activity can indirectly confirm the increase in osteogenic differentiation rates by scaffolds.[119] Alkaline phosphatases (ALPs) are membrane-bound enzymes that hydrolyze monophosphate esters at a high pH (pH 8-10). ALP is secreted by active osteoblasts, the cells responsible for laying down the matrix and mineral during new bone formation in vivo,[116] and involves in initiation of the calcification process. It has been postulated for bone ALP that hydrolyses phosphate esters, resulting in high local phosphate ions (Pi) concentration.[117] The hydrolysis reaction results in the saturation of the extracellular fluid with orthophosphates that induce mineralization.[118]

In this study, ALP activity was measured to investigate the osteogenic differentiation capacity of MSCs cultured onto different PCL substrates and TCP (control sample). For this purpose, MSCs with the density of $5x10^4$ cells/ml were seeded onto the scaffolds as described above (chapter 2.2.1) and cultured for the first three days in standard medium. Three days after cell seeding, the standard medium was removed and osteogenic medium was added (chapter 2.2.4). The osteogenic differentiation on different surfaces was illustrated by ALP production 14, 21 and 25 days after culturing in osteogenic medium and the results are summarized in Fig.39.

As shown in Fig.39, ALP activity increased over time. ALP activity of TCP samples is almost the same for all time points, whereas significant variations are obvious for the three PCL substates. In more detail, at the second and third week of MSCs differentiation, the highest ALP activity was found on high roughness PCL and the lowest on flat PCL. At day 25, optical density of supernatants on low and high roughness PCL is similar and highest than that on flat PCL. Considering that ALP is a marker of osteocytes, these findings prove that MSCs growing on PCL-patterned substrates present higher ability to differentiate into osteocytes. It is worth noting that ALP activity of TCP samples show a significant deviation from that of PCL samples. These findings confirm that topography, and specifically, roughness is above stiffness at modulating MSCs osteogenic induction (see chapter 3.2.5).

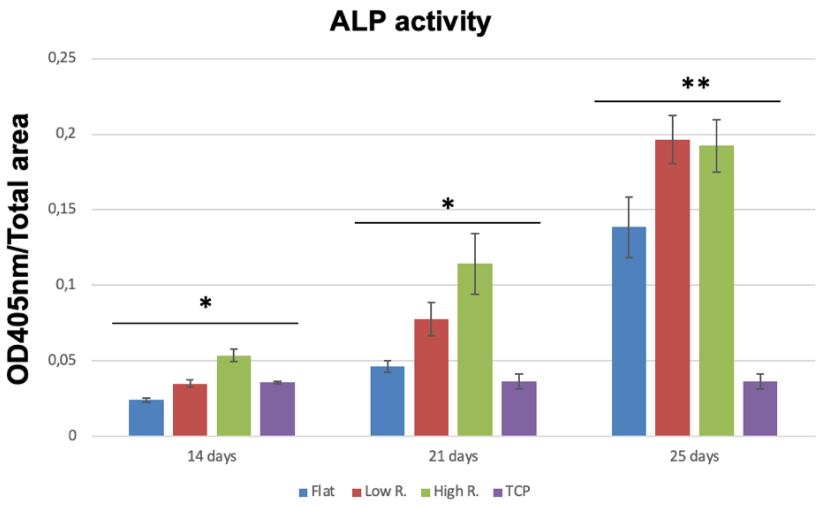

Figure 39: Quantification of the activity of ALP in MSCs grown on flat, low and high roughness PCL and TCP in osteogenic medium at day 14, 21 and 25, normalized by total substrate area (=25mm^2). ALP expression was measured for 10 samples of each substrate group (5 individual experiments) and of each time point in a micro-plate ELIZA reader. The data were subjected to ANOVA with post hoc Tukey HSD test for multiple comparisons between the groups (*p<0.01, **p<0.05).

3.2.7 Quantification of matrix mineralization (Alizarin Red-S)

Biomineralization is the process by which minerals are deposited within or outside the cells of a variety of organisms. The deposited minerals are composed of hydroxyapatite, a calcium phosphate, and are found in the extracellular matrix. Physiological mineralization occurs in hard tissues, like bone, growth-plate cartilage and in dentin, in which several tissue-specific cells are responsible for mineralization. In bone, osteoblasts are responsible for the formation of hydroxyapatite.[120] Mineralization occurs in two steps; It begins with the formation of hydroxyapatite crystals within matrix vesicles, followed by propagation of hydroxyapatite through the membrane into the extracellular matrix.[121]

The mineralization of the extracellular matrix, the last step of the osteogenic differentiation, was evaluated by Alizarin Red-S (ARS) staining after 21 and 28 days of MSCs culture under differentiation conditions (chapter 2.2.6). ARS is a dye that binds to calcium deposits and, so, the appearance of red spots confirms the presence of calcium deposition in the samples and consequently the process of osteogenic differentiation in MSCs. Fig.40 shows representative images of ARS staining at each time point and on different surfaces. It is observed that the number of mineralized nodules increased with the elongation of osteogenic differentiation time. At first glance, we can see that flat PCL has the smallest number of red spots than low and high roughness PCL, but it's not easy to distinguish which substrate has more intensive ARS staining.

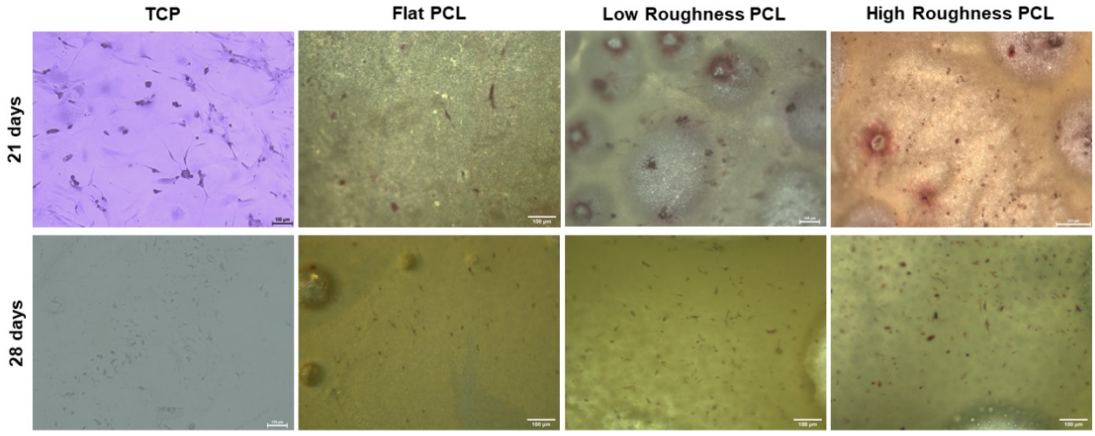

Figure 40: Calcium deposition staining with Alizarin Red-S, 21 and 28 days after culturing of MSCs in osteogenic differentiation medium. Pictures were taken with optical microscope (Leica DM IL Inverted Microscope).

Thus, in order to quantify the mineralization degree of MSCs, the stained calcium deposits were de-stained with cetylpyridinium chloride (CPC), and the optical density (OD) of the extracted stains was measured at 545 nm (Fig.42). At day 21, the highest optical density at 545nm was obtained for MSCs grown on low roughness PCL followed by those on high roughness PCL, with no significant difference. Respectively, at 28 days the highest OD at 545nm was obtained for MSCs grown on high roughness PCL followed by those on low roughness PCL. Furthermore, OD of ARS extractions on PCL substrates have a large deviation compared to that on TCP substrates. Given that the highest OD indicates a higher level of calcium deposits and, therefore, increased matrix mineralization ability, it turns out that MSCs tend to differentiate into osteocytes when they are growing on patterned PCL substrates, and especially on high roughness, than on non-patterned PCL. So, topography and increasing roughness play a significant role at MSCs differentiation.

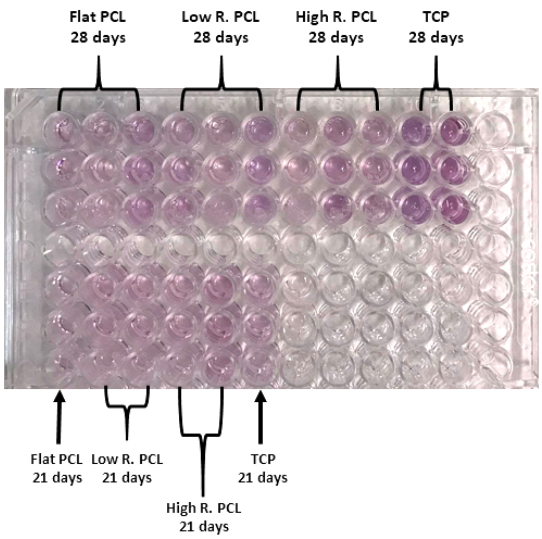

Figure 41: A 96-well plate with the extracted ARS supernatants (random example).

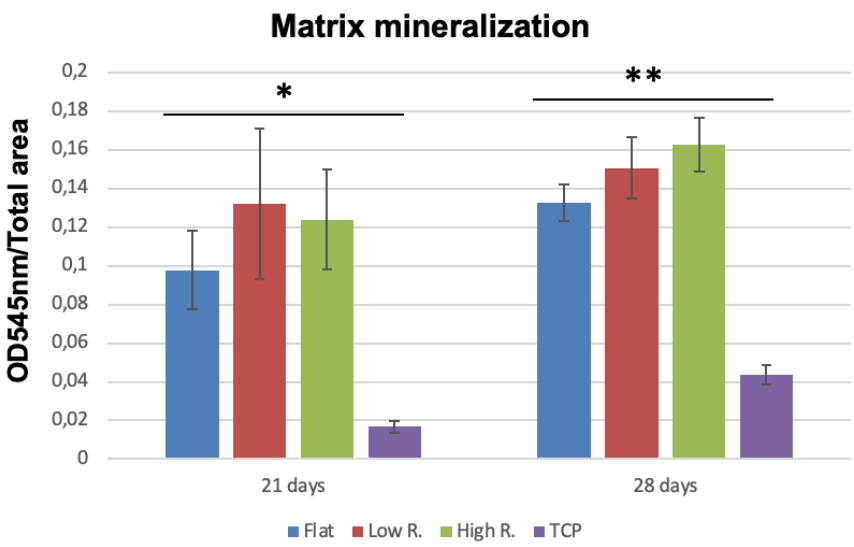

Figure 42: Quantification of the degree of matrix mineralization on flat, low and high roughness PCL and TCP, 21 and 28 days after culturing in osteogenic medium, normalized by total substrate area (=25mm^2). Matrix mineralization was measured for at least 10 samples of each substrate group (5 individual experiments) and of each time point in a micro-plate ELIZA reader. The data were subjected to ANOVA with post hoc Tukey HSD test for multiple comparisons between the groups (*$p<0.05$, **$p<0.001$).

4. Conclusions

In this master thesis defense, we successfully reproduced patterned and non-patterned PCL substrates via soft lithography method, which are used as MSCs cell culture substrates. Ultrafast pulsed laser irradiation was used to fabricate the master/initial topographies. From the physicochemical studies of the PCL substrates, it turned out that the higher the roughness, the higher is the hydrophobic nature. Although the wettability decreases on patterned surfaces, the results show that adhesion and, as such, cell proliferation are favored on these surfaces compared to the non-patterned. This shows that topography plays a more important role in the effect of cellular function than wettability. Therefore, by creating surfaces with topography, we effectively deal with the disadvantage of polycaprolactone's hydrophobic nature.

Results of MSCs adhesion by vinculin expression indicate that cells adhere stronger on low roughness PCL and weaker on flat PCL substrates. These results are related to MSCs proliferation, from which it turned out that cells number on low roughness PCL is almost double than this on flat PCL 7 days after culture. So, it seems that the cells that adhered stronger, proliferated to a greater extent.

Furthermore, it was shown that MSCs shape is affected by topography, as five morphological types (round, star, dendrite, elongated and oblong) appeared. One day after cell culturing, dendrite has the highest occurrence rate on low roughness PCL surfaces, while all morphological types appear on flat and high roughness PCL. Three days after cell culturing, the dendrite is the predominant

morphological type for all the PCL surfaces. Cells respond to extracellular cues by remodeling their cytoskeleton, through which mechanical forces are transmitted to nucleus. Transcriptional co-activators like YAP are transported to the nucleus and are involved to cells mechanoresponse. According to our findings, MSCs seeded on high roughness PCL present higher YAP nuclear/cytoplasmic ratio than cells on TCP, low roughness and flat PCL. Taking into account that TCP is stiffer than PCL (see Tab.5), it turns out that increasing roughness affects stronger than stiffness YAP translocation to nucleus, which signals gene activation for osteogenesis. Thus, we expected higher level of ALP activity and matrix mineralization on high roughness PCL substrates. Indeed, ALP activity was higher on patterned (low and high roughness) PCL substrates than on TCP and flat PCL. These results are consistent with the mineralization process (via Alizarin Red-S), which is increased on high and low roughness PCL substrates.

Summarizing all the above, we could state that micropatterned substrates are able to control MSCs differentiation. Ultrafast laser pulsed irradiation is considered as a simple, precise and effective microfabrication method to produce structures of controlled geometry and pattern regularity. More specifically, the high roughness substrates represented here could be potentially useful in the field of bone tissue engineering, as a supporting matrix providing directed mechanical cues to self-renewal cells, like MSCs, and promoting bone repair.

REFERENCES

1. Dunn, W. A., Schroder, L. A. & Aris, J. P. Historical overview of autophagy. *Autophagy and Cancer* 1–24 (2013) doi:10.1007/978-1-4614-6561-4_1.

2. Gallego, D., Ferrell, N., Sun, Y. & Hansford, D. J. Multilayer micromolding of degradable polymer tissue engineering scaffolds. **28**, 353–358 (2008).

3. Chan, B. P. & Leong, K. W. Scaffolding in tissue engineering: General approaches and tissue-specific considerations. *Eur. Spine J.* **17**, (2008).

4. Chen, F. M. & Liu, X. Advancing biomaterials of human origin for tissue engineering. *Prog. Polym. Sci.* **53**, 86–168 (2016).

5. Hollister, S. J. Porous scaffold design for tissue engineering (vol 4, pg 518, 2005). *Nat. Mater.* **5**, 590 (2006).

6. Agashe, V. & Naik, N. *Biomechanics and Biomaterials in Orthopedics*. *Textbook of Orthopedics and Trauma (4 Volumes)* (2016). doi:10.5005/jp/books/12869_108.

7. Geiger, B., Spatz, J. P. & Bershadsky, A. D. Environmental sensing through focal adhesions. *Nat. Rev. Mol. Cell Biol.* **10**, 21–33 (2009).

8. Hou, Y. *et al.* Surface Roughness and Substrate Stiffness Synergize to Drive Cellular Mechanoresponse. *Nano Lett.* **20**, 748–757 (2020).

9. Higuchi, A., Ling, Q. D., Chang, Y., Hsu, S. T. & Umezawa, A. Physical cues of biomaterials guide stem cell differentiation fate. *Chem. Rev.* **113**, 3297–3328 (2013).

10. Chen, S. *et al.* Colloids and Surfaces B : Biointerfaces Tuning surface properties of bone biomaterials to manipulate osteoblastic cell adhesion and the signaling pathways for the enhancement of early osseointegration. *Colloids Surfaces B Biointerfaces* **164**, 58–69 (2018).

11. D'Sa, R. A., Raj, J., Dickinson, P. J., McCabe, F. & Meenan, B. J. High-Throughput Screening and Hierarchical Topography-Mediated Neural Differentiation of Mesenchymal Stem Cells. *ACS Appl. Mater. Interfaces* **8**, 14920–14931 (2016).

12. Pisani, S. *et al.* Biocompatible polymeric electrospun matrices: Micro–nanotopography effect on cell behavior. *J. Appl. Polym. Sci.* 1–15 (2020) doi:10.1002/app.49223.

13. Khattak, M., Pu, F., Curran, J. M., Hunt, J. A. & D'Sa, R. A. Human mesenchymal stem cell response to poly(ε-caprolactone/poly(methyl methacrylate) demixed thin films. *J. Mater. Sci. Mater. Med.* **26**, (2015).

14. Mano, J. F. *et al.* Natural origin biodegradable systems in tissue engineering and regenerative medicine: Present status and some moving trends. *J. R. Soc. Interface* **4**, 999–1030 (2007).

15. Lu, L. *et al.* In vitro and in vivo degradation of porous poly(DL-lactic-co-glycolic acid) foams. *Biomaterials* **21**, 1837–1845 (2000).

16. Ducheyne, P. *Comprehensive Biomaterials 1st Edition*. *Comprehensive Biomaterials* (2011). doi:10.1016/B978-0-08-055294-1.00060-X.

17. Dave, K. & Gomes, V. G. Materials Science & Engineering C Interactions at sca ff old interfaces : E ff ect of surface chemistry , structural attributes and bioa ffi nity. **105**, (2019).

18. Siddiqui, N., Asawa, S., Birru, B., Baadhe, R. & Rao, S. PCL - Based Composite Scaffold Matrices for Tissue Engineering Applications. *Mol. Biotechnol.* (2018) doi:10.1007/s12033-018-0084-5.

19. Zhang, L. *et al.* Fabrication of alignment polycaprolactone scaffolds by combining use of electrospinning and micromolding for regulating Schwann cells behavior. 1–12 (2018) doi:10.1002/jbm.a.36507.

20. D'Sa, R. A., Burke, G. A. & Meenan, B. J. Protein adhesion and cell response on atmospheric pressure dielectric barrier discharge-modified polymer surfaces. *Acta Biomater.* **6**, 2609–2620 (2010).

21. Griffin, M., Palgrave, R., Baldovino-Medrano, V. G., Butler, P. E. & Kalaskar, D. M. Argon plasma improves the tissue integration and angiogenesis of subcutaneous implants by modifying surface chemistry

and topography. *Int. J. Nanomedicine* **13**, 6123–6141 (2018).

22. Moosazadeh Moghaddam, M. *et al.* Engineered substrates with imprinted cell-like topographies induce direct differentiation of adipose-derived mesenchymal stem cells into Schwann cells. *Artif. Cells, Nanomedicine Biotechnol.* **47**, 1022–1035 (2019).

23. Yang, L., Jurczak, K. M., Ge, L. & van Rijn, P. High-Throughput Screening and Hierarchical Topography-Mediated Neural Differentiation of Mesenchymal Stem Cells. *Adv. Healthc. Mater.* **2000117**, (2020).

24. Gerardo, H. *et al.* Soft culture substrates favor stem-like cellular phenotype and facilitate reprogramming of human mesenchymal stem/stromal cells (hMSCs) through mechanotransduction. *Sci. Rep.* **9**, 1–18 (2019).

25. Yin, Z. *et al.* Electrospun scaffolds for multiple tissues regeneration invivo through topography dependent induction of lineage specific differentiation. *Biomaterials* **44**, 173–185 (2015).

26. Newman, P. *et al.* Relationship between nanotopographical alignment and stem cell fate with live imaging and shape analysis. *Sci. Rep.* **6**, 1–11 (2016).

27. Simitzi, C., Ranella, A. & Stratakis, E. Acta Biomaterialia Controlling the morphology and outgrowth of nerve and neuroglial cells : The effect of surface topography. *Acta Biomater.* **51**, 21–52 (2017).

28. Teo, B. K. K. *et al.* Nanotopography modulates mechanotransduction of stem cells and induces differentiation through focal adhesion kinase. *ACS Nano* **7**, 4785–4798 (2013).

29. Wang, W. *et al.* Involvement of Rac1 in the micro/nano-topography sensing and osteogenic differentiation in bone marrow mesenchymal stem cells. *Mater. Des.* **157**, 402–411 (2018).

30. Niu, H. *et al.* Surface Topography Regulates Osteogenic Differentiation of MSCs via Crosstalk between FAK/MAPK and ILK/β-Catenin Pathways in a Hierarchically Porous Environment. *ACS Biomater. Sci. Eng.* **3**, 3161–3175 (2017).

31. Hou, Y. *et al.* Surface Roughness Gradients Reveal Topography-Specific Mechanosensitive Responses in Human Mesenchymal Stem Cells. *Small* **16**, (2020).

32. Ortiz, R. *et al.* Laser surface microstructuring of a bio-resorbable polymer to anchor stem cells, control adipocyte morphology, and promote osteogenesis. *Polymers (Basel).* **10**, (2018).

33. Wang, Q., Huang, Y. & Qian, Z. Nanostructured surface modification to bone implants for bone regeneration. *J. Biomed. Nanotechnol.* **14**, 628–648 (2018).

34. Abagnale, G. *et al.* Surface topography enhances differentiation of

mesenchymal stem cells towards osteogenic and adipogenic lineages. *Biomaterials* **61**, 316–326 (2015).

35. Wu, Y. N. *et al.* Substrate topography determines the fate of chondrogenesis from human mesenchymal stem cells resulting in specific cartilage phenotype formation. *Nanomedicine Nanotechnology, Biol. Med.* **10**, 1507–1516 (2014).

36. Metavarayuth, K., Lin, Y. & Wang, Q. The Influence of Surface Topographical Cues on the Differentiation of Mesenchymal Stem Cells In Vitro. (2015) doi:10.1021/acsbiomaterials.5b00377.

37. Sousa, I., Mendes, A., Pereira, R. F. & Bártolo, P. J. Collagen surface modi fi ed poly (ε -caprolactone) scaffolds with improved hydrophilicity and cell adhesion properties. vol. 134 (Elsevier, 2014).

38. Steward, A. J. & Kelly, D. J. Mechanical regulation of mesenchymal stem cell differentiation. *J. Anat.* **227**, 717–731 (2015).

39. Metwally, S. & Stachewicz, U. Surface potential and charges impact on cell responses on biomaterials interfaces for medical applications. *Mater. Sci. Eng. C* **104**, 109883 (2019).

40. Khalili, A. A. & Ahmad, M. R. A Review of cell adhesion studies for biomedical and biological applications. *Int. J. Mol. Sci.* **16**, 18149–18184 (2015).

41. Ranella, A., Barberoglou, M., Bakogianni, S., Fotakis, C. & Stratakis, E. Acta Biomaterialia Tuning cell adhesion by controlling the roughness and wettability of 3D micro / nano silicon structures. *Acta Biomater.* **6**, 2711–2720 (2010).

42. You, A., Be, M. A. Y. & In, I. Biomimetic micro / nanostructured functional surfaces for microfluidic and tissue engineering applications. **013411**, (2015).

43. Ribeiro, V. P. *et al.* Influence of different surface modification treatments on silk biotextiles for tissue engineering applications. *J. Biomed. Mater. Res. - Part B Appl. Biomater.* **104**, 496–507 (2016).

44. Tardajos, M. G. *et al.* Chitosan functionalized poly-ε-caprolactone electrospun fibers and 3D printed scaffolds as antibacterial materials for tissue engineering applications. *Carbohydr. Polym.* **191**, 127–135 (2018).

45. Hotchkiss, K. M. *et al.* Titanium surface characteristics, including topography and wettability, alter macrophage activation. *Acta Biomater.* **31**, 425–434 (2016).

46. Tuteja, A. *et al.* Designing superoleophobic surfaces. *Science (80-.).* **318**, 1618–1622 (2007).

47. Song, W., Veiga, D. D., Custódio, C. A. & Mano, J. F. Bioinspired degradable substrates with extreme wettability properties. *Adv. Mater.*

21, 1830–1834 (2009).

48. Alves, N. M. *et al.* Bioinspired superhydrophobic poly(L-lactic acid) surfaces control bone marrow derived cells adhesion and proliferation. *J. Biomed. Mater. Res. - Part A* **91**, 480–488 (2009).

49. Luo, S., Liour, S. & Yu, H. Perfluoro-functionalized PEDOT films with controlled morphology as superhydrophobic coatings and biointerfaces with enhanced cell adhesion w. 4731–4733 (2010) doi:10.1039/c002321c.

50. Chen, F., Lee, C. N. & Teoh, S. H. Nanofibrous modification on ultra-thin poly (e-caprolactone) membrane via electrospinning. **27**, 325–332 (2007).

51. Lim, J. Y. *et al.* Osteoblast Adhesion on Poly (L -lactic Acid)/ Polystyrene Demixed Thin Film Blends : Effect of Nanotopography , Surface Chemistry , and Wettability. 3319–3327 (2005) doi:10.1021/bm0503423.

52. Xu, C., Yang, F., Wang, S. & Ramakrishna, S. In vitro study of human vascular endothelial cell function on materials with various surface roughness. (2004) doi:10.1002/jbm.a.30143.

53. Owen, G. R., Jackson, J., Chehroudi, B., Burt, H. & Brunette, D. M. A PLGA membrane controlling cell behaviour for promoting tissue regeneration. **26**, 7447–7456 (2005).

54. Babaliari, E. *et al.* Engineering cell adhesion and orientation via ultrafast laser fabricated microstructured substrates. *Int. J. Mol. Sci.* **19**, (2018).

55. Schüller-Ravoo, S. *et al.* Microstructured Photo-Crosslinked Poly(Trimethylene Carbonate) for Use in Soft Lithography Applications: A Biodegradable Alternative for Poly(Dimethylsiloxane). *ChemPhysChem* **19**, 2085–2092 (2018).

56. Whitesides, G. M., Ostuni, E., Jiang, X. & Ingber, D. E. S Oft L Ithography in B Iology. *Annu. Rev. Biomed. Eng.* **3**, 335–73 (2001).

57. Su, B., Zhang, A., Meng, J. & Zhang, Z. Soft lithography of ceramic microparts using wettability-tunable poly(dimethylsiloxane) (PDMS) molds. *J. Micromechanics Microengineering* **26**, (2016).

58. Gates, B. D. Nanofabrication with molds & stamps. *Mater. Today* **8**, 44–49 (2005).

59. Qin, D., Xia, Y. & Whitesides, G. M. Soft lithography for micro- and nanoscale patterning. *Nat. Protoc.* **5**, 491–502 (2010).

60. Arango-Santander, S., Pelaez-Vargas, A., Freitas, S. C. & García, C. A novel approach to create an antibacterial surface using titanium dioxide and a combination of dip-pen nanolithography and soft lithography. *Sci. Rep.* **8**, 1–10 (2018).

61. Ntege, E. H., Sunami, H. & Shimizu, Y. Advances in regenerative therapy: A review of the literature and future directions. *Regen. Ther.* **14**, 136–153 (2020).

62. Rajasekaran, R. *et al.* Role of nanofibers on MSCs fate: Influence of fiber morphologies, compositions and external stimuli. *Mater. Sci. Eng. C* **107**, 110218 (2020).

63. Afanasyev, B. V, Elstner, E. E. & Zander, A. R. founder of the mesenchymal stem cell concept Maximow and Friedenstein. *www.ctt-journal.com Cell. Ther. Transplant.* **11**, 35–38 (2009).

64. Galipeau, J. & Sensébé, L. Mesenchymal Stromal Cells: Clinical Challenges and Therapeutic Opportunities. *Cell Stem Cell* **22**, 824–833 (2018).

65. Hao, L. *et al.* Directing the fate of human and mouse mesenchymal stem cells by hydroxyl-methyl mixed self-assembled monolayers with varying wettability. *J. Mater. Chem. B* **2**, 4794–4801 (2014).

66. Almalki, S. G. & Agrawal, D. K. Key transcription factors in the differentiation of mesenchymal stem cells. *Differentiation* **92**, 41–51 (2016).

67. Chaudhary, J. K. & Rath, P. C. Microgrooved-surface topography enhances cellular division and proliferation of mouse bone marrow-derived mesenchymal stem cells. *PLoS One* **12**, 1–22 (2017).

68. Huang, R. *et al.* The topography of fibrous scaffolds modulates the paracrine function of Ad-MSCs in the regeneration of skin tissues. *Biomater. Sci.* **7**, 4248–4259 (2019).

69. Moradi, S. L., Golchin, A., Hajishafieeha, Z., Khani, M. M. & Ardeshirylajimi, A. Bone tissue engineering: Adult stem cells in combination with electrospun nanofibrous scaffolds. *J. Cell. Physiol.* **233**, 6509–6522 (2018).

70. Casagrande, S. *et al.* Biodegradable composite porous poly(dl-lactide-co-glycolide) scaffold supports mesenchymal stem cell differentiation and calcium phosphate deposition. *Artif. Cells, Nanomedicine Biotechnol.* **46**, 219–229 (2018).

71. Mohamadyar-Toupkanlou, F. *et al.* Osteogenic Differentiation of MSCs on Fibronectin-Coated and nHA-Modified Scaffolds. *ASAIO J.* **63**, 684–691 (2017).

72. Núñez-Toldrà, R. *et al.* Dental pulp pluripotent-like stem cells (DPPSC), a new stem cell population with chromosomal stability and osteogenic capacity for biomaterials evaluation. *BMC Cell Biol.* **18**, (2017).

73. Langenbach, F. & Handschel, J. Effects of dexamethasone, ascorbic acid and β-glycerophosphate on the osteogenic differentiation of stem cells in vitro. *Stem Cell Res. Ther.* **4**, (2013).

74. Rutkovskiy, A., Stensløkken, K.-O. & Vaage, I. J. Osteoblast Differentiation at a Glance. *Med. Sci. Monit. Basic Res.* **22**, 95–106 (2016).

75. Birmingham, E. *et al.* Osteogenic differentiation of mesenchymal stem cells is regulated by osteocyte and osteoblast cells in a simplified bone niche. *Eur. Cells Mater.* **23**, 13–27 (2012).

76. Zheng, Z. *et al.* A specific aggregation-induced emission-conjugated polymer enables visual monitoring of osteogenic differentiation. *Bioact. Mater.* **5**, 1018–1025 (2020).

77. Tan, P. S. & Teoh, S. H. Effect of stiffness of polycaprolactone (PCL) membrane on cell proliferation. *Mater. Sci. Eng. C* **27**, 304–308 (2007).

78. Tiaw, K. S. *et al.* Laser surface modification of poly(ε-caprolactone) (PCL) membrane for tissue engineering applications. *Biomaterials* **26**, 763–769 (2005).

79. Pegueroles, M. *et al.* Spatial organization of osteoblast fibronectin matrix on titanium surfaces: Effects of roughness, chemical heterogeneity and surface energy. *Acta Biomater.* **6**, 291–301 (2010).

80. Scott, S., Clouser, C. & Aho, J. Methods to Validate Mesenchymal Stem Cell Quality. *Bio-Techne* 5–6 (2015).

81. Gomzikova, M. O. *et al.* Immunosuppressive properties of cytochalasin B-induced membrane vesicles of mesenchymal stem cells: comparing with extracellular vesicles derived from mesenchymal stem cells. *Sci. Rep.* **10**, 1–13 (2020).

82. Morath, I., Hartmann, T. N. & Orian-Rousseau, V. CD44: More than a mere stem cell marker. *Int. J. Biochem. Cell Biol.* **81**, 166–173 (2016).

83. Yang, M. C. *et al.* The influence of rat mesenchymal stem cell CD44 surface markers on cell growth, fibronectin expression, and cardiomyogenic differentiation on silk fibroin - Hyaluronic acid cardiac patches. *Biomaterials* **31**, 854–862 (2010).

84. Mullen, C. A. *et al.* Cell morphology and focal adhesion location alters internal cell stress. *J. R. Soc. Interface* **11**, (2014).

85. Prasad, A. & Alizadeh, E. Cell Form and Function: Interpreting and Controlling the Shape of Adherent Cells. *Trends Biotechnol.* **37**, 347–357 (2019).

86. Biology, C. Demonstration of mechanical connections between integrins , cytoskeletal filaments , and nucleoplasm that stabilize. **94**, 849–854 (2000).

87. Versaevel, M., Grevesse, T. & Gabriele, S. Spatial coordination between cell and nuclear shape within micropatterned endothelial cells. *Nat. Commun.* **3**, (2012).

88. Gong, T. *et al.* Dynamically tunable polymer microwells for directing mesenchymal stem cell differentiation into osteogenesis. *J. Mater. Chem. B* **3**, 9011–9022 (2015).

89. Matsuoka, F. *et al.* Characterization of Time-Course Morphological Features for Efficient Prediction of Osteogenic Potential in Human Mesenchymal Stem Cells. **111**, 1430–1439 (2014).

90. Matsuoka, F. *et al.* Morphology-Based Prediction of Osteogenic Differentiation Potential of Human Mesenchymal Stem Cells. *PLoS One* **8**, (2013).

91. Olausson, M., Esfahani, N., Östlin, J. & Hägglin, C. Native-born versus foreign-born patients' perception of communication and care in Swedish dental service. *Swed. Dent. J.* **40**, 91–100 (2016).

92. Fomby, P. *et al.* Stem cells and cell therapies in lung biology and diseases: Conference report. *Ann. Am. Thorac. Soc.* **12**, 181–204 (2010).

93. Kelly, D. J. & Jacobs, C. R. The Role of Mechanical Signals in Regulating Chondrogenesis and Osteogenesis of Mesenchymal Stem Cells. **85**, 75–85 (2010).

94. Tanaka-Kamioka, K., Kamioka, H., Ris, H. & Lim, S. S. Osteocyte shape is dependent on actin filaments and osteocyte processes are unique actin-rich projections. *J. Bone Miner. Res.* **13**, 1555–1568 (1998).

95. Fu, R. *et al.* Spreading area and shape regulate apoptosis and differentiation of osteoblasts. *Biomed. Mater.* **8**, (2013).

96. Peng, R., Yao, X. & Ding, J. Effect of cell anisotropy on differentiation of stem cells on micropatterned surfaces through the controlled single cell adhesion. *Biomaterials* **32**, 8048–8057 (2011).

97. Kilian, K. A., Bugarija, B., Lahn, B. T. & Mrksich, M. Geometric cues for directing the differentiation of mesenchymal stem cells. *Proc. Natl. Acad. Sci. U. S. A.* **107**, 4872–4877 (2010).

98. Yang, L. *et al.* Topography induced stiffness alteration of stem cells influences osteogenic differentiation. *Biomater. Sci.* 32–36 (2020) doi:10.1039/d0bm00264j.

99. Gupta, S. K., Li, Y. & Guo, M. Anisotropic mechanics and dynamics of a living mammalian cytoplasm. *Soft Matter* **15**, 190–199 (2019).

100. Case, L. B. *et al.* Molecular mechanism of vinculin activation and nanoscale spatial organization in focal adhesions. *Nat. Cell Biol.* **17**, 880–892 (2015).

101. Li, C. W., Lau, Y. T., Lam, K. L. & Chan, B. P. Mechanically induced formation and maturation of 3D-matrix adhesions (3DMAs) in human mesenchymal stem cells. *Biomaterials* **258**, 120292 (2020).

102. Goldmann, W. H. Role of vinculin in cellular mechanotransduction. *Cell Biol. Int.* **40**, 241–256 (2016).

103. Humphries, J. D. *et al.* Vinculin controls focal adhesion formation by direct interactions with talin and actin. *J. Cell Biol.* **179**, 1043–1057 (2007).

104. Jhala, D. & Vasita, R. A Review on Extracellular Matrix Mimicking Strategies for an Artificial Stem Cell Niche. *Polym. Rev.* **55**, 561–595 (2015).

105. Handorf, A. M., Zhou, Y., Halanski, M. A. & Li, W. J. Tissue stiffness dictates development, homeostasis, and disease progression. *Organogenesis* **11**, 1–15 (2015).

106. Dupont, S. *et al.* Role of YAP / TAZ in mechanotransduction. *Nature* **474**, 179–183 (2011).

107. Niu, L. *et al.* Matrix stiffness controls cardiac fibroblast activation through regulating YAP via AT1R. *J. Cell. Physiol.* **235**, 8345–8357 (2020).

108. Lee, S., Stanton, A. E., Tong, X. & Yang, F. Hydrogels with enhanced protein conjugation efficiency reveal stiffness-induced YAP localization in stem cells depends on biochemical cues. *Biomaterials* **202**, 26–34 (2019).

109. Loye, A. M. *et al.* Regulation of Mesenchymal Stem Cell Differentiation by Nanopatterning of Bulk Metallic Glass. *Sci. Rep.* **8**, 1–11 (2018).

110. Ghasemi, H. *et al.* Tissue stiffness contributes to YAP activation in bladder cancer patients undergoing transurethral resection. *Ann. N. Y. Acad. Sci.* **1473**, 48–61 (2020).

111. Kurotsu, S. *et al.* Soft Matrix Promotes Cardiac Reprogramming via Inhibition of YAP/TAZ and Suppression of Fibroblast Signatures. *Stem Cell Reports* **15**, 612–628 (2020).

112. Zonderland, J. & Moroni, L. Steering cell behavior through mechanobiology in 3D: A regenerative medicine perspective. *Biomaterials* **268**, 120572 (2021).

113. Rosa, D. S. *et al.* Evaluation of the Thermal and Mechanical Properties of and Their Blends. *J. Appl. Polym. Sci.* **91**, 3909–3914 (2004).

114. Eshraghi, S. & Das, S. Mechanical and microstructural properties of polycaprolactone scaffolds with one-dimensional, two-dimensional, and three-dimensional orthogonally oriented porous architectures produced by selective laser sintering. *Acta Biomater.* **6**, 2467–2476 (2010).

115. Cosgrove, B. D. *et al.* Nuclear envelope wrinkling predicts mesenchymal progenitor cell mechano-response in 2D and 3D microenvironments. *Biomaterials* **270**, 120662 (2021).

116. Birmingham, E. *et al.* OSTEOGENIC DIFFERENTIATION OF MESENCHYMAL STEM CELLS IS REGULATED BY OSTEOCYTE AND OSTEOBLAST CELLS IN. **23**, 13–27 (2012).

117. Correia, C. R. *et al.* Semipermeable Capsules Wrapping a Multifunctional and Self-regulated Co-culture Microenvironment for Osteogenic Differentiation. *Nat. Publ. Gr.* (2016) doi:10.1038/srep21883.

118. Golub, E. E. & Boesze-Battaglia, K. The role of alkaline phosphatase in mineralization. *Curr. Opin. Orthop.* **18**, 444–448 (2007).

119. Rostami, F., Tamjid, E. & Behmanesh, M. Drug-eluting PCL/graphene oxide nanocomposite scaffolds for enhanced osteogenic differentiation of mesenchymal stem cells. *Mater. Sci. Eng. C* **115**, 111102 (2020).

120. Faia-Torres, A. B. *et al.* Osteogenic differentiation of human mesenchymal stem cells in the absence of osteogenic supplements: A surface-roughness gradient study. *Acta Biomater.* **28**, 64–75 (2015).

121. Kecerdasan, I. & Ikep, P. No 主観的健康感を中心とした在宅高齢者における 健康関連指標に関する共分散構造分析Title. 6.